

**CHARACTERIZATION OF PLASMA EXPOSED
AISb BILAYER THIN FILM**

**Dissertation Submitted to the Bharathiar University
in partial fulfillment of the requirement
for the award of the degree of**

**MASTER OF PHILOSOPHY
IN
PHYSICS**

Submitted by

**Mr. T. Abdul Kareem, M. Sc.,
(Reg. No: 2006 R 672)**

Under the guidance of

Dr. A. ANU KALIANI, M. Sc., M. Phil., Ph. D.



**Department of Physics
Kongunadu Arts and Science College (Autonomous)
Coimbatore – 641 029**

September – 2007

CERTIFICATE

This is to certify that the dissertation entitled "CHARACTERIZATION OF PLASMA EXPOSED AISb BILAYER THIN FILM" submitted to the Bharathiar University, in partial fulfilment of the requirements for the award of the Degree of **Master of Philosophy in Physics** is a record of original research work done by **Mr. Abdul Kareem. T** during the period September 2006-September 2007 of his study in the **Department of Physics** at Kongunadu Arts and Science College (Autonomous), Coimbatore, under my supervision and guidance and the dissertation has not formed the basis for the award of any Degree / Diploma / Associateship / Fellowship or other similar title to any candidate of any university.

A. Anu Kaliani
27/9/07

Signature of the Guide

(Dr. A. ANU KALIANI)
Dr. A. ANU KALIANI M.Sc., M.Phil., Ph.D.
Lecturer
Department of Physics,
Kongunadu Arts and Science College,
G. N. Mills (PO)
COIMBATORE - 641 029.

Countersigned



Dr. A. Subbarayan

Head of the Department
Dr. A. SUBBARAYAN
M.Sc., M.Phil., Dip. Edu. P.H.D.,
READER & HEAD
Department of Physics,
Kongunadu Arts & Science College,
COIMBATORE - 641 029.

Dr. A. A. Sivakumar

Principal
Dr. A. A. SIVAKUMAR.
M.Sc. Ph.D., M. Ed., PGDEE,
PRINCIPAL
Kongunadu Arts & Science College,
COIMBATORE - 641 029.

DECLARATION

I **ABDUL KAREEM. T** hereby declare that the dissertation entitled, "**CHARACTERIZATION OF PLASMA EXPOSED AISb BILAYER THIN FILM**" submitted to the Bharathiar University, in partial fulfilment of the requirements for the award of the Degree of **Master of Philosophy** is a record of original research work done by me during September 2006-September 2007 under the supervision and guidance of **Dr. A. ANU KALIANI**, Lecturer, Department of Physics, Kongunadu Arts and Science College (Autonomous), Coimbatore -29 and it has not formed the basis for the award of any Degree / Diploma / Associateship / Fellowship or other similar title to any candidate of any university.

Place: Coimbatore

Date: 27.09.07



Signature of the Candidate

Mr. Abdul Kareem.T

CERTIFICATE

ACKNOWLEDGEMENT

In the name of God, most gracious, most merciful, praise be to God, the cherisher and sustainer of the worlds, who appeared in front of me in many forms and suggestions, encouragement and generous assistance given by them have influenced me to complete my research work before the stipulated time and it would be impossible to thank them all individually here. But I express my gratitude to every one for their kind heart.

I place on records my deepest sense of gratitude to my respectful guide **Dr. A. Anukaliani**, M.Sc, M.Phil., Ph.D., Lecturer in Physics (Kongunadu Arts and Science College, Coimbatore), for her constant encouragement, guidance and meticulous support to my research work.

My profound thanks to management, Secretary **Dr. M. Aruchami**, M.Sc., BT., Ph.D., FAZ., FRES. (Lond.), **Dr. A. A. Sivakumar**, M.Sc., Ph.D., FSESc., (Principal) and **Dr. A. Subbarayan**, M. Sc., M. Phil., Ph. D., Dip. Ed. (Reader and Head, Department of Physics) for giving necessary facilities and permitting me to do the study.

I am particularly indebted to **Mr. S. Inbakumar**, Research Scholar, and to my colleague **Mr. M. J. Balu**, M. Phil Scholar, Department of Physics (Kongunadu Arts and Science College, Coimbatore) for their benevolence, suggestions and encouragement during this work.

I would like to express my special thanks to **Mr. M. Matheswaran**, Research Scholar, Department of Physics, for his kind heart and the help done for coating the bilayer thin film.

My sincere thanks to **Mr. B. Anandavel**, B. E., Lecturer in Foundry Technology, PSG College of Technology, Coimbatore, for his generosity and his fervent help on XRD studies of the materials.

I am extremely thankful to **Mr. N. Muthukumarasamy**, M.Sc., M.Phil., Senior Grade Lecturer and **Mr. K. Sakthivel**, M.Sc., Senior Grade Lecturer, Department of Physics, Coimbatore Institute of Technology, Coimbatore, for their skilled and enthusiastic help on optical absorption studies of the samples.

I express my deep sense of gratitude and continue to remain obliged to **Dr. K. Bindu**, M. Sc., M. Phil, Ph. D., Post Doctoral Fellowship (Department of Solar Energy Materials, Universidad Nacional Autonoma de Mexico, Mexico), **Dr. T. H. Muhammed Shahin**, M. Sc, Ph.D., Post Doctoral Fellowship (University of Pisa, Italy), **Mr. S. Natarajan**, M. Sc., M. Phil., Dip. Ed., **Dr. N. Easwaran**, M. Sc, M. Phil., Ph. D., Reader in Physics, **Dr. T. Balasubramaniam**, M. Sc, M. Phil., Ph. D., B. Ed., Reader in Physics, **Dr. R. Sathyamoorthi**, M. Sc., M. Phil., Ph.D., PGDCA., **Dr. M. Dhanam**, M. Sc, M. Phil., Ph. D., Reader in Physics, **Dr. R. Sarojini**, M. Sc., M. Phil., Ph. D., **Mr. K. Rajasekar**, M. Sc., M. Phil., B. Ed., **Ms. L. Kungumadevi**, M. Sc., M. Phil., PGDCA, **Mr. R. Dharmaraaj**, M. Sc., and **Ms. B. Maheswary**, M. Sc., Department of Physics, Kongunadu Arts and Science College, who provided the necessary help when and

wherever needed and for their kindness, suggestions, encouragement, moral support, ideas and good wishes in executing this work.

My sincere thanks to **Mr. K. Muthukumar**, M. A., M. Phil. Lab Assistant and to other non teaching staffs, Department of Physics, Kongunadu Arts and Science College.

I am grateful to express my profound and sincere thanks to **Mr. S. Chandramohan, Mr. A. Saravanan, Mr. P. Sudakar, Mr. R. V. Sathish kumar** (Research Scholars) and to all the staff members in the Department of Physics, Kongunadu Arts and Science College, for their encouragement and co-operations.

I feel happy to thank my colleagues **Ms. S. Geetha, Ms. Neetha Jose, Sr. Jessy Mathew. N, Ms. Dheera. P. Devasia, Ms. B. Punithaveni, Mr. T. M. Sathyadevan, Mr. Ranjith G. Nair** and to my friend **Mr. P. G. Sajesh**, M.Sc, B.Ed, M.Ed. for their help at various levels of my work.

I cherish to acknowledge the benevolence of my parents, brother, sisters and friends for their constant love, encouragement, enthusiasm, blessings, co-operation and support during the entire course of study. Peace be upon us.

Abdul Kareem. T

CONTENTS

| | | |
|-----------|---|----|
| Chapter 1 | Introduction | 1 |
| Chapter 2 | Literature Review | 5 |
| Chapter 3 | Thin Film Preparation | 9 |
| | 3.1 Introduction | 9 |
| | 3.2 Thin Film Deposition Technique | 9 |
| | 3.3 Vacuum Coating Unit | 11 |
| | 3.4 Substrate | 12 |
| | 3.5 Sample Preparation | 13 |
| Chapter 4 | Plasma | 14 |
| | 4.1 Introduction | 14 |
| | 4.2 Plasma Temperature | 15 |
| | 4.3 Types of Plasma | 16 |
| | 4.4 Gas Discharge | 17 |
| Chapter 5 | Thin film Modification Using Cold Plasma | 22 |
| | 5.1 Introduction | 22 |
| | 5.2 Principle of Plasma Treatment | 23 |
| | 5.3 Experimental Setup | 23 |
| Chapter 6 | Characterization of Plasma Exposed Thin Film | 25 |
| | 6.1 Introduction | 25 |
| | 6.2 Structural Parameters | 25 |
| | 6.2.1 Results and Discussion | 29 |
| | 6.3 Optical Properties | 32 |
| | 6.3.1 Results and Discussion | 35 |
| Chapter 7 | Conclusion | 40 |
| | References and Bibliography | 41 |

CHAPTER 1

INTRODUCTION

Plasma is the most common form of matter, so, it is often called the fourth state of matter. It is distinct from other lower energy states of matter, solid, liquid, and gas, although it is closely related to the gas phase in that it also has no definite form or volume. It is interesting to study the action of plasma on the other three states of matter.

In a neutral gas each atom has the same number of negatively charged electrons orbiting its nucleus as positively charged protons inside the nucleus, while such a gas may possess plenty of chemical activity along with dynamical effects like fluid turbulence; it shows little response to electric and magnetic fields and is practically unable to conduct electricity. The ionization can take place either because the gas is very hot or subjected to some outside source of energy. The resulting plasma consists of interpenetrating and interacting clouds of freely roaming positive and negative charges whose motions both generate electromagnetic fields and are in turn influenced by them, but without sufficient sustaining power, plasma recombine into neutral.

The important characteristics of plasma are temperature and density which range from relatively cool and tenuous like aurora to very hot and dense like the central core of a star. A gas becomes plasma when the kinetic energy of the gas particles rises to a value equal to the ionization energy of the gas. When this level is reached collisions of the gas particles cause a rapid cascading ionization, resulting in plasma. If necessary energy is provided by heat, the threshold temperature is from

50,000 K – 1, 00,000 K and the temperature for maintaining plasma ranges up to hundreds of millions of degree.

Plasma can be accelerated and steered by electric and magnetic fields which allows it to be controlled and applied. Plasma research is yielding a greater understanding of the universe and it also provides many practical uses, new manufacturing technique, consumer products and the prospect of abundant energy.

Plasma processing of multilayer thin film

The advances in our understanding of physics and chemistry of ionized gases has led to the widespread adoption of plasma technology for the deposition and removal or etching of thin films as well as for the modification of surfaces in a diverse variety of technologies. Microelectronic applications have been the main technological driver in this regard. In addition, there are critical plasma processing operations in the automotive, optical coating, biomedical, information recording, waste management and aerospace industries.

There are three important interfaces in semiconductor device technology, such as semiconductor-semiconductor, metal-semiconductor and oxide-semiconductor interface. In the semiconductor-semiconductor interface or p-n junction, where one side of the interface is doped with acceptor type impurities and the other side with donor type impurities. The second type metal-semiconductor interface is an extremely important one because of two reasons. First, electrical contact must be made to the semiconductor device to operate it, and these contacts almost always involve a metal- semiconductor interface. In this type, which is an ohmic contact, the metal semiconductor interface must offer minimum resistance to current flow in either direction over a wide temperature

range. Second, another type of metal-semiconductor interface can be made which offer low resistance to one direction of current flow and very high resistance to the opposite direction of current flow. Such a contact is commonly called a Schottky Barrier and has a wide use as fast switch or for protecting circuit elements from high voltage transients [1].

An important consequence of low temperature diffusion and the resulting inter layer interactions is the instability produced in SBDs (Schottky Barrier Diodes). Schottky diodes are solid-state devices formed by placing a metal in intimate contact with a lightly doped semiconductor. These devices find many applications in the semiconductor industry example as ‘clamps’ to prevent transistors from going into saturations, and as discrete devices in logic and memory arrays. The disadvantage of using SBDs is that the electrical characteristics are extremely sensitive to the conditions of the interface between metal and semiconductor. Contaminations, oxide layers and or metallurgical reactions at this interface can cause major variations in diode behavior [1]. The Al-Sb bilayer diffused film becomes SBD because one side of it is made up of metal and other side is semiconductor.

Present Work

This dissertation is dealt with the effect of plasma on thin films and also to study whether an Al-Sb bilayer thin film exposed to plasma forms a compound or not. Thin film plays a dominant role in modern technology due to their numerous and powerful applications: rectifiers, transistors, photoelectric devices, magneto meters, solar cells, lasers, super conducting elements and so forth. An essential criterion of thin film structures in these applications is that they maintain structural integrity.

In bilayer and their inter diffusion, the inter diffusion or reaction on the bulk scale can generally be ignored. This is not the case for thin film structures where pronounced reaction or inter diffusion can occur over these distances even at room temperatures. It is only recently that experimental techniques have been available to determine mass transport on this scale [1, 2].

Here, the electron temperature of cold plasma is about 100 eV (10^6 K) but the ambient temperature is nearly 373 K which is measured by a thermo couple. When a bilayer thin film of a semiconductor is exposed to the above two temperatures and to the fast moving electrons and ions in the plasma, the plasma can modify the properties of the thin film and it roughens the surface also by etching.

In this dissertation, Chapter 2 deals with the literature survey done for supporting our work. Chapter 3, Chapter 4 and Chapter 5 deals with the methods of thin film preparation, plasma production methodology and the thin film modification using cold plasma. Characterization of thin film is discussed in the Chapter 6 and conclusion is given in Chapter 7.

CHAPTER 2

LITERATURE REVIEW

The discovery of semiconductors is one of the greatest scientific and technological breakthroughs of the 20th century and it has changed the civilization itself. The semiconductors have been the subject of very intensive research over recent decades because of their applications in various electro-optical devices.

Al-Sb thin film sample selected to be treated with plasma which is a semi-conducting compound; with energy band gap of 1.62eV and it is a highly efficient solar material. Many studies have been done on the Al-Sb compound thin films to make it as a reliable material for solar energy tapping. Al-Sb in thin film form is used to construct room temperature detectors, infrared detectors, infrared lasers and high-speed oscillators, such as Resonant Tunneling Diodes (R T Ds) with switching speeds approaching tera-hertz frequencies. The properties of these devices are highly dependent on the barrier thickness and it is sensitive to atomic scale variations in the morphology of the interfaces and composition caused by diffusion and or inter-mixing during growth [3, 4].

There are some major technical problems in growing Al-Sb crystals and fabricating devices on its basis. They are mainly related to with the intrinsic nature of Al, its high reactivity or affinity to oxygen and high volatility of Sb. Normally Al-Sb is synthesized by co-melting a mixture of Al and Sb with a given stoichiometry, but the properties of Al-Sb thin films vary with composition due to its variation while vacuum

evaporation. The stack elemental layer deposition and their intermixing can form a well-defined composition of Al-Sb thin film [5].

R.K. Mangal et al [5] have studied the intermixing by rapid thermal annealing. They have confirmed the variation in intermixing of interfaces from the optical absorption spectra, where the absorption increases in the case of vacuum annealed and rapid annealed films when compared to as deposited films. They have showed that the Rapid Thermal Annealing (RTA) treated samples giving better mixing effects and the band gap approaches to the bulk value. The samples with thickness ratio Sb: Al: 1:3 for both types of treated samples shows the band gap value of the bulk Al-Sb semiconductors, which suggests the formation of single phase at the interface due to mixing of Al and Sb.

They have used Rutherford Back Scattering Spectrometry (RBS) to explain intermixing of bi-layer. In the case of vacuum annealed and RTA, the peak shifted towards higher energy side and the intensity of the peak reduced, which is the result of mixing effect in binary system. Better mixing effects are observed in RTA film when compared to vacuum annealed film.

M. Singh et al [6] performed isochronal heat treatment of bilayer for inter-diffusion. The electrical resistivity studies show an increasing resistance due to the mixing of Al and Sb in each other. This change in resistance indicates possible formation of granularity in the system. The films initially show positive temperature coefficient of resistance (TCR) suggesting metallic behavior up to temperature 320 K, and further increasing concentration of Al in Sb is due to larger diffusion coefficient of Al in Sb and shows negative TCR which indicates semi conducting behavior.

The absorption spectra of swift heavy ion irradiated samples show a sharp absorption edge around 700nm. R.K. Mangal et al [7] suggests that this variation in absorption spectra is due to the variation in intermixing at the surface, and the mixing occurs due to thermal heating. They have confirmed the inter-diffusion from the RBS spectrum also. The X-ray diffraction study of the ion irradiated Al-Sb sample indicates the formation of crystalline Al-Sb compound.

D.K. Avasthi et al [8] have performed an online study on swift heavy ion beam induced mixing at interface and this study revealed that the mixing depends on the electronic excitation. Another study conducted by Ratnesh Gupta et al [9] shows that the energy deposited in multilayer is in the form of electronic excitation during ion irradiation, which results modifications at the interface and the interfacial roughness also increased in the system.

M. Singh and Y. K. Vijay [10] measured the I-V characteristics and magneto resistance of Al-Sb thin films with Cu electrode as electrical contact. They have found that IV characteristics are non-linear and magneto resistance decreases in case of annealed Al-Sb thin film due to inter-diffusion.

The study of irradiation effect of 350 MeV Au⁺ ions on Ti/Si multilayer conducted by V. Sisodia et al [11] showed damage at the interface with the absence of a continuous fringe pattern in X-ray reflectivity (XRR) patterns at high fluence doses in comparison to the pristine interface. It is also revealed that the intermixing is attributed to energy deposited by the incident ions in the electronic system of the target.

The above literatures reveal that the intermixing is occurring due to the thermal heating and the energy deposition in the multilayer is in the form of electronic excitation. This gives a possibility of introducing the bilayer thin films in plasma.

Plasma treatment is a powerful and a versatile way to modify surface properties and obtain materials with improved properties. L.Von Muhlen et al [12] treated amorphous nitrogen-incorporated carbon thin films (a-C: H (N)) with plasma and they showed that the wettability of the film could be altered by modifying its surface roughness and also by incorporating functional groups.

From the survey of literature, it can be seen that almost no attempt has been made to study the properties of plasma exposed Al-Sb thin films. In the present work we have made an effort to understand the properties of plasma exposed Al-Sb thin film.

CHAPTER 3

THIN FILM PREPARATION

3.1 Introduction

Thin film science has got tremendous attention because of their numerous applications in diverse fields such as electronic industries, space science, military weapon systems, solar energy utilization, high memory computer elements, and sensors and also in microelectronics [13, 14].

Thin films can be considered to possess two dimensions. Commonly a film can be explained as a homogeneous solid material contained between two parallel planes and extended infinitely in two directions but restricted along the third direction [14]. In other words, thin film can be explained as any solids or liquid with one of its dimension very much less than of the other two [15].

The thin film properties such as physical, electrical and optical are strongly determined by the method of deposition, rate of deposition, substrate temperature, environmental conditions, residual gas pressure, purity of the material and structural and compositional variations [1, 14].

3.2 Thin film deposition techniques

Thin film can be prepared from a variety of material such as metals, semiconductors, insulators or dielectric etc. and for this purpose various techniques have been employed. These techniques have a characteristic effect on the nucleation and growth of a thin film and thereby on its physical properties [1, 16, 17, and 18].

The steps involved in thin film formation are

1. Creation of atomic or molecular or ionic species.
2. Transport of these species through a medium.

3. Condensation of the species on a substrate.

The deposition process can be broadly classified into two, namely, chemical methods and physical methods.

Chemical methods

Among the chemical and electrochemical methods the most important are electrolytic deposition, electroless deposition, anodic oxidation and chemical vapor deposition [19].

In cathode electrolytic deposition the substance to be deposited is present in a solution or melts in the form of ions. The properties of the deposited film as its adhesion to the substrate and its crystal structures are influenced by the composition of the electrolyte.

Electroless deposition involves the deposition from the solution by electrochemical process without the presence of an externally applied field. The rate of deposition depends on the temperature of the bath and in some cases the deposition needs to be stimulated by a catalyst. But, anodization is field-assisted form of thermal growth [20].

Chemical Vapour Deposition (CVD) is a widely used method and involves essentially, exposure of the substrate to one or several vaporized compounds or reagent gas, some or all of which contain constituents of the desired substance to be coated. A chemical reaction is then initiated at or near the substrate surface producing the desired material as solid phase reaction product, which condenses on the substrate [15, 21].

Physical methods

The most important physical methods for the preparation of thin films are sputtering and vacuum evaporation. Both methods require lowered pressure in the working space and therefore use of vacuum techniques is made.

1. Sputtering technique

The process of ejection of atoms from the cathode surface by impinging energetic positive ions of noble gases such as helium, argon, neon and krypton, at a reduced pressure under a high DC voltage gives rise to the sputtering phenomenon [17, 22].

2. Vacuum evaporation

The most widely used method for the preparation of thin films is the vacuum evaporation. This method is comparatively simple, but it can provide films of extreme purity and of pre-selected structure only under proper experimental conditions.

The process of film formation by evaporation consists of several physical stages, including, transformation of the material to be deposited by evaporation or sublimation into the gaseous state, transfer of atoms or molecules from the evaporation source to the substrate, deposition of these particles on the substrate and rearrangement or modifications of their binding on the surface of the substrate.

The rate of condensation or deposition of the vapor atoms depends on the vapor- source- substrate geometry and the condensation coefficient on the surface under given physical conditions. The dissociation or association or both the association and dissociation processes usually accompany vaporization of alloys and compounds. The tendency to dissociate is greater with higher evaporation temperatures and lower pressure [18].

3.3 Vacuum coating unit

The vacuum coating unit used in this experiment is the “HIND HIVAC” coating unit (12A4D), which is shown in Figure 3.1, which

consists of three main sections namely, the vacuum chamber, the pumping system, and the electrical equipment with connection.

A three-stage oil diffusion pump can evacuate the vacuum chamber backed by a double stage gas ballast rotary pump capable of evaluating 200 liters/minutes. The silicon oil DC704 is having a low vapor pressure (10^{-9} torr) and have been used as the charge for the diffusion pump.

The chamber pressure could be measured from a thermal conductivity gauge (pirani gauge) for low pressure ($0.5-10^{-3}$ torr) and an ionization gauge (penning gauge) for still lower pressures ($10^{-3}-10^{-6}$ torr). The evaporation of the material from the filament or boat has been facilitated by an LT supply obtained from the secondary of a transformer.

3.4 Substrate

The function of the substrate is to provide the base on to which the thin film circuits are fabricated and various thin film multi-layers are deposited. The most widely used substrates for polycrystalline films are glass, fused silica, beryllium oxide based ceramics, aluminum nitride and metals.

Cleaning of the substrate is an inevitable process in thin film coating. The proper cleaning technique depends on the nature of the substrate, the nature of the contaminations and the degree of cleanliness required. Cleaning involves the breaking of adsorption bonds between the substrate and the contaminants without damaging the substrate surface itself. The energy to perform this step may be provided directly as heat or ion bombardment by chemical reaction or by mechanical scrubbing [15].

Cleaning of glass substrate

The glass substrates used here were first treated with sodium hydroxide (Na OH) solution. This alkaline agent dissolves fatty materials

by saponification and menders them wet. Then the substrates are washed by hand using a cotton pad and a solution of a detergent. The substrates were then rinsed in distilled water and placed in an ultrasonic cleaner where they were agitated for 30 minutes in a solution of detergent and distilled water. Again a second agitation in distilled water followed, and the substrates were dried in a hot air oven. Finally, the substrates were pre-cleaned with isopropyl alcohol and then heated in a hot air oven for about one hour at a temperature of 100°C.

3.5 Sample preparation

The high purity Aluminium (99.99%) thin foils and pure Antimony (99.5%) have been obtained from Sigma Aldrich Chemicals, USA to prepare Al-Sb bilayer thin films. Bilayer structure of Al-Sb was deposited onto a glass substrate by thermal evaporation method at a pressure of 10^{-6} torr using HIND HI VACUUM Coating unit. The glass substrates were placed in the substrate holder above the boats carrying material. The bilayer of AlSb thin films were prepared by stack elemental method. Antimony (1000Å) is coated first to avoid oxide formation in the middle of the bilayer and later Aluminium (2250Å) is coated over the Antimony film.

Thickness measurement

The thickness of the film is very small which gives rise to properties different from those of bulk material. Therefore, film thickness is a very important parameter for basic investigations as well as for film applications. Here the thickness of the film was measured by employing a digital quartz crystal thickness monitor. The Sb layer has thickness 1000 Å and the Al has thickness 2250 Å on the glass substrate. Then the prepared samples were exposed to glow discharge plasma.

CHAPTER 4

PLASMA

4.1 Introduction

Most of the visible matter in the universe exists as ionized gas, or plasma, such as in stars and interstellar gas clouds. Plasma is found in lightning bolts, the Aurora Borealis and the ionosphere surrounding our planet. They also have applications such as in lighting, surface processing and the quest for fusion energy. Plasmas are tending to be very hot because collision energies of the order of an electron volt are required to break neutral atoms and molecules into free electrons and ions [23].

Plasma is an ionized gas and is usually considered to be a distinct phase of matter. The free electric charges make the plasma electrically conductive so that it couples strongly to electromagnetic fields. This fourth state of matter was first identified by Sir William Crookes in 1879 and dubbed the name “Plasma” by Irving Langmuir in 1929[24].

In any gas there is always a small degree of ionization. But any ionized gas cannot be called as plasma; “plasma” is quasi-neutral gas of charged and neutral particles, which exhibits collective behavior [25]. Plasma consists of free electrons, radicals, ions, UV radiations and various highly excited neutral and charged species independent of the gas used [26]. It is a conducting gas, i.e., a gas that contains a noticeable proportion of charged particles (electron and ions).

The main difference between a neutral gas and an ionized gas or a plasma arises due to the fact that where as in case of an ionized gas the externally applied electric or magnetic field has little effect on its

properties, plasma is profoundly affected by either an electric or a magnetic field or by the simultaneous presence of both these fields. The electrons become strongly heated when moving in the electric field and receiving energy from it [27].

In plasma instead of the single species of particles as in a gas, we have at least three types of particles such as electrons, positive ions, and neutral molecules [28]. It is a collection of charged particles sufficiently dense that space charge effects can result in strongly coherent behavior [29].

Plasma consists of a mixture of neutral particles, positive ions (atoms or molecules that have lost one or more electrons) and negative electrons. Plasma is conductor of electricity, but a volume with dimensions greater than the so-called Debye length exhibits electrically neutral behavior. At a microscopic level, corresponding to distances shorter than the Debye length the particles of plasma do not exhibit collective behavior but instead react individually to an electric field.

Because of the large difference in mass, the electrons come to thermodynamic equilibrium among themselves much faster than they come into equilibrium with the ions or neutral atoms. For this reason the ion temperature may be very different from the electron temperature [24].

4.2 Plasma temperature

The effective or characteristic temperature T associated with a given energy E is simply given by $T=E/k_B$, k_B is the Boltzmann constant. For $E=2eV$, the electrons have an amazing high temperature of some 23000K, However, because there are so few of them, their heat content is small and the chamber walls do not heat appreciably. Neutral gas atoms or molecules and ions are far less energetic; the former have energies of

only 0.025eV or $T=293\text{K}$ and the latter, energies of $\sim 0.04\text{eV}$ or $T=500\text{K}$. Ions have higher energies than neutrals because they acquire energy from the applied electric field.

The electron temperature for an applied voltage of 350 V is determined as 4.06×10^6 K and the ambient temperature measured is 100°C by a thermocouple.

4.3 Types of plasma

There are thermal plasma and non-thermal plasma based on the relative temperature of electrons, ions and neutrals. Thermal plasmas have electrons and the heavy particles at the same temperature, i.e., they are in thermal equilibrium with each other. Non-thermal plasma, on the other hand have ions and neutrals at a much lower temperature (room temperature) where as electrons are much hotter.

There are three types of plasma namely 1) high pressure or thermal or equilibrium plasmas 2) low-pressure or cold or non-equilibrium plasma which include glow discharges and 3) ultra cold plasma.

1. High pressure / Thermal plasma / Equilibrium plasma

Plasma that approaches a state of Local Thermal Equilibrium (LTE) has thermal energy content and temperature around 10^4K with electron densities ranging from 10^{21} m^{-3} to 10^{26} m^{-3} and are normally called as hot plasma. Unique properties associated with thermal plasmas are namely high energy density, high thermal conductivity, variable electrical conductivity and high emission of radiation. Thermal plasma technologies have been widely used for material processing such as plasma spraying, plasma metallurgy, plasma cutting and hazardous waste treatment. High intensity arcs, plasma torches or RF discharges at high pressures ($p > 75$ torr) are used to produce thermal plasma.

2. Low pressure / Cold plasma / Non-equilibrium plasma

The cold plasmas are characterized by high electron temperature (1-10eV) compared to the temperature of heavy particles and plasma densities are typically in the range of 10^8 m^{-3} to 10^{18} m^{-3} . The key features of low-pressure plasmas are the production of active species (from inert species) and their capability to cause physical and chemical reaction at relatively low gas temperatures. Cold plasma is produced by a DC glow discharge or by an RF discharge. The low pressure plasma processing is being used for microelectronic industry, efficient lighting and surface modification of materials. This is an extremely interesting technology employed largely in an empirical basis at present, which will benefit a great deal from the rapidly growing science base [25].

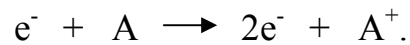
3. Ultra Cold Plasma

It is possible to create ultra cold plasmas, by using lasers to trap and cool neutral atoms to temperature of 1mK or lower. Another laser then ionizes the atoms by giving each of the outermost electrons just enough energy to escape the electrical attraction of its parent ion. The key point about ultra cold plasmas is that by manipulating the atoms with lasers, the KE of the liberated electrons can be controlled. Using standard pulse lasers, the electron energy can be made to correspond to a temperature as low as 0.1K, a limit set by the frequency bandwidth of the laser pulse. The ions, however, retain the milli-Kelvin temperature of the neutral atoms [30].

4.4 Gas Discharge

The applications of a sufficiently high DC voltage between metal electrodes immersed in a low-pressure gas initiate a discharge. The discharge reflects a gaseous breakdown that may be viewed as the

equivalent of dielectric breakdown in an insulating solid; the dielectrics conduct electricity at critical applied voltage. In gases the process begins when a stray electron near the cathode carrying an initial current i_0 is accelerated toward the anode by the applied electric field (E). After gaining sufficient energy, the electron collides with a neutral gas atom (A) converting it into a positively charged ion (A^+). During this impact ionization process, charge conservation indicates that two electrons are released, that is



These are accelerated and now bombarded onto two additional neutral gas atoms, generating more ions and electrons, and so on. Meanwhile, the electric field drives ions in the opposite direction where they collide with the cathode, ejecting, secondary electrons. This also undergoes charge multiplication. Until a sufficiently large avalanche current is produced which ultimately causes the gas to breakdown.

In order for breakdown to occur, the distance 'd' between electrodes must be large enough to allow electrons to incrementally gain the requisite energy from an ionization cascade. The electrodes must be wide enough to prevent the loss of electrons or ions through sideways diffusion out of the inter-electrode space. The Townsend equation,

$$i = \frac{i_0 e^{(\alpha d)}}{[1 - \gamma (e^{\alpha d} - 1)]} \quad \text{----- 4.1}$$

The equation reveals that the discharge current 'i' rises dramatically from 'i₀' because of the combined effects of impact ionizations and secondary electron generation. These processes are

respectively defined by constants ‘ α ’ and ‘ γ ’, known as the Townsend ionization coefficients, where the ‘ α ’ represents the probability per unit length of ionization occurring during an electron-gas atom collision. The constant ‘ γ ’ is the Townsend secondary electron emission coefficient and is defined as the number of secondary electron of charge ‘ q ’ traveling a distance ‘ λ ’. The probability of reaching the ionization potential ‘ V_i ,

$$V_i = e^{-(V_i / (q E \lambda))} \quad \text{-----4.2}$$

so that

$$\alpha = \frac{1}{\lambda (e^{-V_i / (q E \lambda)})} \quad \text{----- 4.3}$$

where ‘ λ ’ is the inter collision distance or mean free path in a gas.

Breakdown is assumed to occur when the denominator

$$[1 - \gamma (e^{\alpha d} - 1)] = 1 \quad \text{-----4.4}$$

for then the current is infinite. Then the Paschen’s Law, is expressed as

$$V_b = \frac{A p d}{\ln (P d) + B} \quad \text{----- 4.5}$$

where A and B are constants.

At low values of ‘ $P d$ ’ there are few electron-ion collisions and the secondary electron yield is too low to sustain ionization in the discharge. On the other hand, at high pressures there are frequent collisions, and since electrons do not acquire sufficient energy to ionize gas atoms, the discharge is quenched. Thus at either extreme, ion generation rates are low and high-voltages are required to sustain the discharge. In between, at typically a few hundred to a thousand volts the discharge is self-sustaining. This means that for each electron at the cathode, $e^{(\alpha d)}$

electrons reach the anode and the net effect of collisions is to produce a new electron at the cathode.

In the Townsend discharge, a tiny current flows initially due to a small number of charge carriers in the system. With charge multiplication, the current increases rapidly, but the voltage is limited by the impedance of the power supply remains constant, eventually, when enough electrons produce sufficient ions to regenerate the same number of initial electrons, the discharge becomes self-sustained. The gas begins to glow now and the voltage drops accompanied by a sharp rise in current. At this point normal glow occurs. Initially, ion bombardment of the cathode is not uniform but concentrated near the cathode edges or at other surface irregularities. As more power is applied, the bombardment increasingly spreads over the entire surface until a nearly uniform current density is achieved. A further increase in power results in both higher voltage and cathode current density levels. The abnormal discharge regime has now been entered and this is the operative domain for sputtering and other discharge processes such as plasma etching.

At still higher currents, the cathode gets hotter. Now thermionic emission of electrons exceeds that of secondary-electron emission and low voltage arcs propagates. Arcs have been defined as a gas or vapor discharges where the cathode voltage drop is of the order of the minimum ionizing or excitation potential. Furthermore, the arc is a self-sustained discharge that supports high currents by providing its own mechanism from electron emission from negative or positive electrodes.

In the DC discharge, there is a progression of alternating dark and luminous region between the cathode and anode, where the Aston dark space is very thin and contains both low energy electrons and high-energy

positive ions, each moving in opposite directions. Beyond it the cathode glow appears as a highly luminous layers that envelopes and clings to the cathode. De-excitation of positive ions through neutralization is a probable mechanism of light emission here. Next to appear is the important Crookes or cathode dark space where some electrons are energized to the point where they begin to impact-ionize neutrals, other lower energy electrons impact neutrals without ion production. This region is dark because of the relatively little ionization. Most of the discharge voltage is dropped across the cathode dark space, also commonly referred to as cathode sheath. The resulting electric field serves to accelerate ions toward their eventual collision with the cathode. Next aligned one is the negative glow. Here the visible emission is apparently due to interactions between assorted secondary electrons and neutrals with the assisting excitation and de-excitation. Beyond this are the faraday dark space, the positive column, and finally the anode.

When a DC voltage 'V' is applied between the anode and cathode the electric potential distribution, unlike the case for a simple vacuum capacitor, is highly nonlinear with distance x; similarly, the electric field ($\xi = - d (V) / d (x)$) is not constant. Further more, the deviations are most distinct near the electrodes. These characteristics stem from the complex distribution of charge near electrodes and within the plasma, and the resultant current they produce.

CHAPTER 5

THIN FILM MODIFICATION USING COLD PLASMA

5.1 Introduction

Last decade has witnessed a tremendous surge interest regarding various techniques for material surface preparations and modifications. The critical principle behind these technologies is that they make it possible to change the surface properties of a material without changing the bulk properties. This essentially creates ‘new’ materials with new possibilities, opening novel perspective to help to resolve production or design issues and develop innovative applications. Production difficulties frequently arise when a new material is substituted for an existing one and turn out to have surface characteristics that are incompatible with effective processing. Recent surface modifications methods often can address such problems while also inspiring unanticipated design solution as designers begin to think beyond conventional mechanical or chemical surface alteration. One such process is low-pressure plasma technology, an environmental friendly and cost effective way to modify material surfaces on a microscopic level without manual operations or the use of chemical products.

Low temperature plasma is an ionic gas whose components and characteristic are different from the normal gas. Plasma of different ionization extents can be produced with the help of an electrical discharge. Since the temperatures of plasma are relatively low, the active species in plasma easily lose their energy once reacting with the material. It has been used in a wide variety of engineering applications. It is also

used in a controlled and reproducible way to clean, activate, etch or otherwise modify the surface of plastics, metals or ceramic materials including the textile processes to improve their bonding capabilities or achieve totally new surface properties.

5.2 Principle of plasma treatment

The plasma atmosphere consists of free electrons, radicals, ions, UV radiations and lots of different excited particles in dependence of the gas used. Different reactive species in the plasma chamber interact with the substrate surface. Cleaning, modification and coating are depending on plasma parameters.

Further more, the plasma process can be carried out in different manners.

1. The substrate can be treated directly in the plasma zone.
2. The substrates can be positioned outside the plasma; this process is called remote process.
3. The substrate can be activated in the plasma followed by a subsequent grafting.
4. The substrate can be treated with a polymer solution or gas, which will be fixed or polymerized by a subsequent plasma treatment.

5.3 Experimental setup

The plasma chamber used in this experiment is cylindrical made up of stainless steel which is shown in Figure 5.1, which consists of three segments namely the cylindrical chamber, the vacuum pumping system, and the power supply.

The cylindrical chamber is 50 cm in length and 25 cm in diameter with four view ports which helps to see what happens inside the chamber.

The diffusion pump can evacuate the chamber and bring the vapor pressure up to 4.5×10^{-3} mb. The chamber pressure could be measured by

a thermal conductivity gauge (pirani gauge) for low pressure ($0.5-10^{-3}$ torr) and still lower pressures can be measured using a penning gauge.

The chamber was cleaned by acetone and the copper electrodes were placed through either side of the cylindrical chamber and connected to the DC power supply. Then each sample was placed inside the plasma chamber using a stainless steel sample holder with coated surface facing the cathode.

The electrode distances have been fixed to be 5cm apart and the sample placed 2cm apart from the cathode. Then the chamber was firmly closed and the vacuum pump was switched on. After reaching the required pressure (0.2 mb) inside the chamber, the power supply was switched on and voltage of 350V was applied between the electrodes.

Three thin film samples of Al-Sb (2250Å-1000 Å) were chosen (A, B, and C) and exposed to plasma for 20 minutes, 30 minutes and 60 minutes respectively for the above mentioned plasma parameters. The samples D and E were annealed in 100°C and 200°C for 60 minutes to compare the results with plasma exposed films.

CHAPTER 6

CHARACTERIZATION OF PLASMA EXPOSED THIN FILM

6.1 Introduction

The optical and electronic properties of thin films are very sensitively influenced by the crystallographic and micro-structural characteristics of the film. Similarly, the electronic behavior of the photovoltaic junction is also affected strongly by the structural features of the interface at the junction [18].

Most modern characterization techniques for thin film structural and compositional analysis are scattering techniques. Scattering methods are particularly well suited for thin film analysis since they tend to have high sensitivity, so that the amount of material needed for analysis is small and both structural and compositional information can be obtained.

In scattering techniques, usually a beam of photon, X-rays, electrons or charged particles is incident on the specimen surface. The incident beam interacts with the solid sample and gives rise to scattered beams, the scattered beams also will be in the form of photon, X-Rays, electron and charged particles. By analyzing the scattered beams, structural as well as compositional information of the thin film sample can be obtained such as XRD, TEM, SEM, and RBS.

6.2 Structural parameters

About 95% of all solid materials can be described as crystalline. When X-rays interact with a crystalline substance, we get diffraction patterns. Each and every crystalline substance gives the same pattern

always and in a mixture of substance each produces its pattern independently of the others.

In the crystalline structure, the atoms are arranged in a regular pattern, and the smallest volume element is called a unit cell. The axes a , b , c and the angles between them α , β and γ describe the dimensions of the unit cell.

When an X-ray beam hits an atom, the electrons around the atom starts to oscillate with the same frequency as the incoming beam. In almost all directions we get destructive interference. But in the case of crystal the atoms are arranged in a regular pattern and in very few directions we get constructive interference. The waves will be in phase and there will be well-defined X-ray beam leaving the sample at various directions. Hence, a diffracted beam may be defined as a beam composed of a large number of scattered rays reinforcing on another.

The X-rays are reflecting from a series of parallel planes of the crystal and the orientation and the inter-planar spacing of these planes are defined by three integers h , k and l which cut the 'a' axis of the unit cell in ' h ' sections, the 'b' axis in ' k ' sections and the 'c' axis in ' l ' sections. A zero indicates that the planes are parallel to the corresponding axis.

The XRD method can provide the following types of information.

1. The kinds of material that compose a solid (qualitative analysis)
2. The quantities of materials that compose the solid (quantitative analysis).
3. The quantities of materials that are crystallized (crystallinity).
4. The amount of stress present in the solid (residual stress).
5. The size of crystallites that compose the solid (crystallite size).

6. Average orientation of crystallites that compose the solid (Texture).

Analysis of the diffraction patterns and comparisons with standards ASTM or JCPDS or ICDD data can reveal the existence of different crystallographic phases in the film, the relative abundance, the lattice parameters, and any preferred orientation. From the width of the diffraction line, it is possible to estimate the average grain size in the film [31].

From the XRD profile, the inter-planar spacing ' d_{hkl} ' was calculated using Bragg's relation, which describes the condition for constructive interference for X-ray scattering from atomic planes of a crystal.

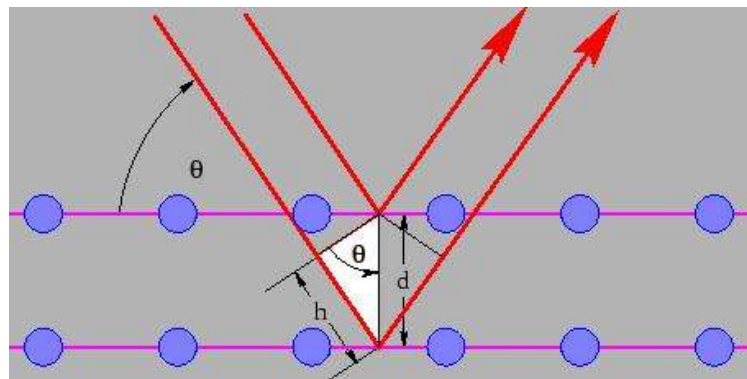


Figure 6.1 Bragg's law from crystal plane

From the Figure 6.1,

$$d_{hkl} = n \lambda / 2 \sin \theta \text{ (m)} \quad \text{----- 6.1}$$

where ' d ' is the distance between the atomic planes parallel to the axis of the incident beam, ' θ ' is the angle of incidence relative to the planes, ' n ' is the order of the reflection and ' λ ' is the wavelength of X-ray.

The crystal size (D) is calculated using the Scherrer's formula from the Full Width Half Maximum (FWHM), which explains how the width of a Bragg reflection increases with decreasing crystal size,

$$D = k \lambda / \beta \cos \theta \text{ (m)}. \quad \text{----- 6.2}$$

where 'k' is the shape factor ≈ 0.94 , ' λ ' is the wavelength of the X-rays (1.5406Å for Cu K_{α}), ' θ ' is the Bragg's angle and ' β ' is the FWHM.

Micro strain and dislocations play a prominent role in the various distortions of the crystal lattice. In the vicinity of dislocations, the atoms reside on equilibrium positions distinct from those in the unperturbed lattice and cause the surrounding bond length to contract and expand. The strain fields introduced by dislocation may extend over many hundreds of unit cells in the crystal. The inter-planar spacing 'd' is thus subjected to a variation and may not be accounted for by a fixed value ' d_0 ', but by a distribution of 'd' values. The strain fields thus cause a smearing of scattered X-ray intensity around ' d_0 ' and broadening of radiation. These strain fields are denoted as micro strain; because they appear on a length scale that is small when compared with the inverse linear attenuation coefficient ' $1/\mu$ ' [32]. The dislocation density (δ) can be calculated from the relation

$$\delta = 1/ D^2 \text{ (m}^{-2}\text{)}. \quad \text{---- 6.3}$$

The dislocation density is a measure of how many dislocations are present in a quantity of a material. Since a dislocation is a line defect, the dislocation density is defined as the total length of dislocation per unit volume (m^{-2}). It is the number of dislocation lines intersecting a unit area.

The origin of the micro strain is related to the lattice misfit, which in turn depends upon the deposition conditions. The micro strain (ϵ) can be calculated from the following relation

$$\epsilon = (\beta \cos \theta / 4). \quad \text{----- 6.4}$$

Experimental process

The X-ray diffraction experiment requires an X-ray source, the sample under the investigation and a detector to pick up the diffracted X-rays. The X-ray radiation most commonly used is that emitted by Copper, whose characteristic wavelength for 'K_α' radiation is 1.5406 Å. When the incident beams strikes the sample, diffraction occurs in every possible orientation of 2θ. The diffracted beam is detected by using a moveable detector such as Geiger counter, which is connected to a chart recorder.

In this experiment, 'Shimadzu model XRD 6000(LabX)' is used and the counter is set to scan over a range of 2θ values (10 deg – 80 deg) with a scan speed of 5 deg/min.

6.2.1 Results and discussion

From the XRD analysis, inter planar distance, miller indices (hkl), crystal size, dislocation density and micro strain were calculated and tabulated for each sample (samples A, B, and C exposed to plasma for 20 min, 30 min and 60 min respectively and sample D annealed for 60 min at 473K) and is shown in Table 6.2 to Table 6.7 and also the XRD patterns for these samples are shown in Figure 6.2 to Figure 6.9.

It is observed from the XRD graph that the peaks are due to the formation of AlSb crystals and the observed lattice parameters obtained in good agreement with the JCPDS values. There are two types of AlSb crystal structures observed in the plasma treated samples AlSb in Cubic and in orthorhombic structures which may be due to the presence of electrons and ions in the plasma. The electrons and ions are not at the same temperature (measure of kinetic energy) in cold plasma. The temperature of electron is high compared to the temperature of ions.

The intensity of major peaks of Al and Sb changes in plasma exposed and annealed samples. This change in intensity of major peaks of Al and Sb is due to mixing of bilayer system. A similar effect for swift heavy ion irradiated sample was also observed by R. K. Mangal et al [7].

As deposited and plasma exposed samples

Figure 6.2 shows the XRD pattern of as deposited sample and the data are tabulated in Table 6.2A and 6.2B. From the Table 6.2A it is seen that the highest peak for Al is at 37.7816 in the plane (111) and other peaks are for Sb. There are no peaks for AlSb compound in as deposited sample. The calculated ' d_{hkl} ' and cell parameters (Table 6.2B) of Al and Sb are in good agreement with the JCPDS data. The intensity of Al is 21 counts as seen from the XRD graph (Figure 6.2) and the highest peak of Sb is at 22.94 in (003) plane and its intensity is 10 counts.

Figure 6.3 shows the XRD pattern of plasma exposed film for 20 minutes and its data are tabulated in Table 6.3A and in Table 6.3B in the Figure 6.3B peaks for AlSb at 29.15 and 41.36 are for cubic structure and peaks at 34.38 is for orthorhombic structure. Tabulated ' d_{hkl} ' and cell parameters of AlSb are in good agreement with the JCPDS values. Here the intensity of Al is reduced to 10 from 21 and intensity of Sb is increased from 10 to 26 when compared to as deposited sample. The decrease in intensity of Al is due to the diffusion of Al in to the Sb film.

Figure 6.4 shows the XRD patterns of plasma exposed sample. This sample exposed to plasma for 30 minutes and the calculated data are tabulated in Table 6.4A and Table 6.4B. From figure 6.4, it is seen that AlSb peaks are present at 25.1046, 51.8950 are for cubic structure and 34.5433, 73.2500 are for orthorhombic structure. The tabulated data of ' d_{hkl} ' and cell parameters (Table 6.4A and Table 6.4B) matches well with

the JCPDS data. The intensity of Sb is increased from 10 to 22 counts when compared to as deposited sample but decreased by 4 points from sample A. This decrease in the intensity counts may be because of the imperfection in mixing. The absence of Al peaks is due to the fact that the Al has diffused in to Sb and AlSb compound formation has taken place at the interface of the two layers. The increase in intensity of Sb is due to the diffusion of Al in to Sb. The intensity variation of Sb itself indicates that the mixing of the two layers has taken place. The confirmation of cell parameters of AlSb proves the formation of AlSb compound at the interface of the two layers.

Figure 6.5 shows the XRD pattern of AlSb bilayer thin film exposed to plasma for 60 minutes. The intensity of Al is reduced from 21 to 7 and that of Sb increased from 10 to 60 when compared to as deposited sample. This intensity variation of Al and Sb compared to as deposited sample is due to the mixing of these two layers. Table 6.5A shows ' d_{hkl} ' values of the newly formed compounds and the peaks were found at 29.17 and 51.794 for AlSb cubic and 33.18 and 34.88 for AlSb orthorhombic structure. Tabulated ' d_{hkl} ' and cell parameters are in good agreement with the JCPDS values which confirms the mixing of these two layers at the interface and the formation of compound also.

As deposited and annealed samples

The XRD pattern of annealed sample is given Figure 6.6 and it shows a peak at 34.53 for AlSb orthorhombic structure. The ' d_{hkl} ' values and cell parameters (Table 6.6A and 6.6B) also confirms the presence of AlSb in the annealed sample. The intensity at 38.3880 of Al is 53, which is increased much from the as deposited sample (intensity at 37.7816 of Al is 22 counts) but the value of FWHM shows that the grain size of Al is

decreased. The peak at 23.5016 is of Sb (intensity is 23 counts) and it is also greater than the as deposited value (intensity at 22.94 is 10 counts) but the FWHM of the Sb peaks of annealed sample shows that the grain size of Sb is increased after annealing. This effect may be due to the bonding of neighboring atoms and forming AlSb compound. The increase in intensity of the predominant peak of Sb indicating the higher degree of preferential orientation towards this direction.

6.3 Optical properties

Thin films are widely used which demands the accurate knowledge of the optical properties of the films. Discrepancies in the optical behavior of films have been attributed to their physical state viz, crystalline or otherwise, in-homogeneity, compositional deviations etc. The optical study of solid concerns not only the physical phenomena but also the interaction of photon energy with matter and the consequent changes in the electronic states.

The reflection, transmission and absorption studies helps to evaluate the optical constants such as absorption edge, optical energy band gap, optical transitions which may be direct or indirect, allowed or forbidden transitions refractive index n , absorption index or extinction coefficient ' k ', and absorption coefficient ' α ' and also of the nature of the solid material [14, 22].

Absorption of light by different materials can induce various types of transitions such as band to band, between sub-bands, between impurity levels and bands, interactions with free carriers within a band, resonance due to vibration state of lattice and impurities. These lead to the appearance of bands or absorption peaks in the absorption spectra. Hence

the spectral positions of bands determine the type of transitions occurring during the process.

Absorption of light by semiconductor takes place broadly by two processes namely, 1) by raising the electrons from the valence band to the conduction bands or 2) by exciting the lattice vibrations of the materials or both by photon energy.

In the case of metals, free electrons contribute mostly to the optical processes. But in an insulator or an intrinsic semiconductor it is the bound electron in the valence band, the contribution of which prevails. In the absence of any thermal energy only possible absorption that can take place is when the incident radiations of sufficient energy excites valence electrons across the forbidden energy band gap into the conduction band. The resulting absorption spectrum is however, a continuum of intense absorption at the short wavelength having more or less a steep absorption edge.

From Bouger's law, the intensity of radiation 'I' is generally attenuated in an exponential form, $e^{(-\alpha t)}$, i.e.,

$$I = I_0 e^{(-\alpha t)} \quad \text{----- 6.5}$$

where ' α ' is the absorption coefficient and 't' is thickness of the sample. So,

$$\alpha = 2.303 \log(I_0/I)/t \quad \text{-----6.6}$$

and ' α ' is related to the extinction coefficient ' k_f ' by

$$k_f = \alpha \lambda / 4 \pi \quad \text{-----6.7}$$

The absorption coefficient of a material indicates how far light having a specific wavelength or energy can penetrate the material before being absorbed. A small absorption coefficient means that light is not readily absorbed by the material. The absorption coefficient of a solar cell

depends on two factors, namely the material making up the cell and the wavelength or energy of the light being absorbed. Solar cell material has an abrupt edge in its absorption coefficient. The reason is that the light of energy below the material's band gap cannot free an electron and it is not absorbed.

In a crystalline or poly-crystalline material both direct or indirect optical transitions are possible depending on the band structure of the material. Assuming parabolic bands, the relation between absorption coefficient ' α ' and band gap energy ' E_g ' for a direct transition is (Mott and Davis 1979)

$$\alpha h \nu = \text{constant} (h \nu - E_g)^n \quad \text{-----6.8}$$

and for indirect transition by

$$\alpha h \nu = \frac{A (h \nu - E_g + E_p)^n}{\exp(\theta_D/T) - 1} + \frac{B (h \nu - E_g - E_p)^n}{1 - \exp(-\theta_D/T)} \quad \text{---6.9}$$

where ' E_p ' is the phonon energy assisting the transition, ' θ_D ' is the Debye temperature and A, B are constants, ' E_g ' is the energy band gap, ' ν ' is the frequency of the incident radiation and ' h ' is the Planck's constant. The magnitude of the exponent ' n ' depends on the type of transition and takes the value 1/2, 3/2, 2 and 3 for direct allowed, direct forbidden, indirect allowed and indirect forbidden transitions respectively.

The usual method of determining band gap is to plot a graph between ' $(\alpha h \nu)^{1/n}$ ' and ' $h \nu$ ' and look for that value of 'n' which gives best linear graph in the band edge region. Obviously, there will be a single linear region in direct transition and two linear portions in indirect transitions [34].

Experimental process

The transmittance of the samples was analyzed from 190 nm to 2500 nm by 'JASCO V-570' UV-Vis Spectro-Photometer. This spectrophotometer was connected to a computer and the absorbance spectrum was obtained by using a specific software tool.

6.3.1 Result and discussion

From the absorption spectra (Figure 6.7 to Figure 6.12), it is seen that the absorption is varying for the treated and annealed samples from the as deposited sample. The variation in absorption is may be due to the AlSb crystal formation.

The metal aluminum has high reflectivity therefore the absorption should be small and the presence of absorption edge means the formation of the semiconductor. But when the film was exposed to plasma, the plasma etches and roughens the surface of the film; this will increase the scattering of incident light. This is the reason for the non uniform variation of absorption in the plasma exposed samples.

The electron temperature, ion temperature and the ambient temperature inside the chamber brings mixed effects and this may be the reason for the formation of the non uniform grains of Al and Sb. The

formations of AlSb crystals were already confirmed from the XRD analysis dealt in section 6.2.

Band gap is the amount of energy expressed in electron volts (eV) required to kick an electron from a semiconductor's valance band which is full of electrons bound to the atoms into its empty conduction band where electrons are free to move. Photons with energy lower than the band gap energy escape unabsorbed and photons with higher energy are absorbed.

The AlSb is intrinsically better than Ge, Si and CdTe which are essentials for high energy photon detector [35] and AlSb is an indirect band semiconductor. Therefore the band gap of the samples were measured by drawing a graph of photon energy ($h\nu$) vs $(\alpha h\nu)^{1/2}$. The semimetal Sb has a negative band gap (i.e. the top of the valence band is higher than the bottom of the conduction band in energy) and it transmits almost all the light incident on it and the absorption is about zero, which is shown in Figure 6.7.

Al of thickness of 2250 Å is coated over the transparent Sb thin film. The absorption spectra of the bilayer film is given in Figure 6.8 which shows that there is a transmission below 700 nm because of the reflection effect of aluminum where lower energies are reflected more and higher energies were penetrated through the sample.

Figure 6.9A shows an absorption edge at 700 nm for plasma treated sample (20 minutes). The band gap energy found from Figure 6.9B is 1.60 eV. It is the band gap energy of AlSb compound, which

confirms the presence of AlSb at the interface of the bilayer thin film after plasma treatment.

The absorption spectra shown in Figure 6.10A for the sample treated for 30 minutes shows an absorption edge near 700 nm. The band gap energy of the sample is 1.88 eV (Figure 6.10B). Only the metal Al and Sb are present here and this band gap energy comes close to the bulk value (1.62 eV) of AlSb. Therefore it can be concluded that the band gap energy 1.88 eV is due to the formation of AlSb compound at the interface of Al and Sb bilayer film.

Absorption edge nearly at 700 nm in the absorption vs wavelength graph plotted in Figure 6.11A for plasma treated sample for 60 minutes shows formation of a semiconductor in the sample. The band gap energy calculated (Figure 6.11B) is 2.4 eV. The building block of the sample is Al and Sb and the absorption in this range comes close to the semiconductor AlSb.

Another sample is annealed for 60 minutes at 473 K in 10^{-3} torr vacuum. A graph is plotted between absorption vs wavelength (Figure 6.12A) shows an absorption edge near 690 nm and the band gap calculated (Figure 6.112B) is 1.32 eV. This band gap shows the presence of AlSb due to the intermixing of Al and Sb bilayer thin film.

The variation in the absorption is due to the mixing of Al and Sb at the interface and also due to the variation in intermixing interface with exposure time or it may be due to the etching effect of plasma. Plasma treated sample for 20 minutes shows a band gap energy of 1.60 eV and other plasma exposed films and vacuum annealed film shows band gap

very close to bulk value of AlSb, i.e., 1.62 eV. The absorption of electromagnetic energy in this range in the metal Al-Sb bilyer film formed may be due to the formation of AlSb semiconductor at the interface.

The results obtained are in well agreement with the works done by R. K. Mangal *et al* in rapid thermal annealing [5] and in swift heavy ion irradiated [7] sample. Plasma treated samples given better mixing effect and the band gap energy approaches to the bulk value, which is in good agreement with the above literatures [5, 7].

Table 6.7, shows that the grain size of newly formed AlSb compound is decreased with increase in treatment time, which is due to the etching effect of plasma. The decrease in grain size is the reason for the increase in band gap energy with increase in plasma exposure time.

It is also seen that dislocation density and micro-strain are increasing with decreasing grain size of AlSb compounds in plasma treated samples. The dislocation density and micro strain on the AlSb compound is higher in annealed film when compared to plasma-exposed samples, which is due to the better mixing of Al and Sb in plasma exposed sample.

The effect of plasma and annealing on thin film is different. The difference is well understood from the formation of two types of crystal structures in plasma treated sample and homogeneous crystal formation in annealed film which is shown in Table 6.7 (when the sample were annealed only orthorhombic crystals of AlSb formed and no cubic structures). This difference is also seen from the dislocation density of the

samples while analyzing the grain size and band gap energy. More research will bring out the secret of these two effects on the crystals.

The solar spectrum consists of photons from 0.5 eV to 4 eV. The variations in band gap of the same material for various plasma exposure time reveals that the plasma can be used to modify the physical and surface properties of thin films and it can be used to tune a particular band gap for a specific material.

The formation of AlSb crystal in the plasma exposed AlSb bilayer thin film can be explained by the thermal spike model [33]. In the thermal spike model one assumes first thermalization of the electronic system within some 10-14 s and an energy transfer to the lattice via electron-phonon coupling within a few 10-12 s. Depending on the material and the energy deposited by the ions and the electrons, the temperature in the surroundings of the ions and electron path may significantly exceed the melting point and a liquid cylinder of some nano meter in diameter is formed, which subsequently and is rapidly quenched to the ambient temperature within few tens to a few hundreds of pico seconds. Due to the high cooling rate, a non equilibrium material is left in the track. Such a transient increase of temperature within a very small local volume is often called a 'thermal spike'. This mechanism results in atomic transport across the interfaces of a plasma exposed layer system.

CHAPTER 7

CONCLUSION

In our achievement in producing the III-V semiconductor AlSb holds promise for low cost and ambient-temperature radiation detection. The XRD patterns and optical absorption studies also confirms the formation of AlSb crystals in plasma exposed samples.

To produce electronic devices, quality single crystals of AlSb require crystal purity and stoichiometry. While Al and Sb are commercially available in pure states, they both aggressively react with air. The III-V liquid state also reacts with most crucible materials, leading to contamination of the melt during crystal growth. The relatively high vapor pressure of Sb leads to non-stoichiometry in as-grown crystals. Such technical challenges have deterred fully developing an AlSb system for electronic devices. We have achieved a separate processing breakthrough, allowing us to obtain un-doped crystals of AlSb. Processing optimization is expected to produce crystals of AlSb suitable for gamma ray detection at room temperature and solar cells of AlSb active to all energies of the solar spectrum.

More research should be done on this field to develop a plasma system to manufacture the AlSb crystals for solar cells and radiation detectors. The advantage of developing the plasma system is that the tuning of band gap of the material for a particular range and this leads to a reduction in the time for annealing.

REFERENCE

1. George Has and Rudolf E. Thun, *Physics of thin films*, Academic Press, NY & London, 2, (1964).
2. Sapoval, B., Hermann, C., *Physics of semiconductors*, Springer, (2004).
3. Nosho, B. Z., Weinberg, W. H., Zinck, J. J., Shanabrook, B. V., Bennet, B. R. and Whitman, L. J., *Structure of InAs/AlSb/InAs resonant tunneling diode interfaces*, J. Vac. Sci. Technol., B16, 4, 2381-2386, (1998).
4. Kutny, V. E., Rybka, A. V., Abyzov, A. S., Davydov, L. N., Komar, V. K., Rowland, M. S., and Smitg, C. F., *AlSb single-crystal grown by HPBM*, Nucl. Instrum. & Meth. Phys. Res., A458, 448-454, (2001).
5. Mangal, R. K., Tripathi, B., Singh, M. and Vijay, Y. K., *Study of annealing effects in AlSb bilayer thin films*, Bull. Mater. Sci., 30, 1, 5-7, (2007).
6. Singh, M., Arora, J. S., Vijay, Y. K. and Sudharshan, M., *Optical, electrical and thermoelectric power studies of AlSb thin film bilayer structure*, Bull. Mater. Sci., 29, 1, 17-20, (2006).
7. Mangal, R. K., Singh, M., Vijay, Y. K. and Avasthi, D. K., *Preparation of AlSb semiconductor by swift heavy ion irradiation*, Bull. Mater. Sci., 29, 7, 653-657, (2006).
8. Avasthi, D. K., Assmann, W., Nolte, H., Mieskes, H. D., Huber, H., Subramaniam, E. T., Tripathi, A. and Ghosh, S., *On-line study of ion beam induced mixing at interface by swift heavy ions*, Nucl. Instrum. & Meth. Phys. Res., Sec.B., 156, 143-147, (1999).
9. Ratnesh Gupta, Ajay Gupta, Avasthi, D. K., Principi, G. and Tosello, *Effects of swift heavy ion-irradiation on Cr/Fe/Ni multilayers*, Nucl. Instrum. & Meth. Phys. Res., Sec.B., 156, 153-157, (1999).

10. Singh, M. and Vijay, Y. K., *Magneto-resistance and I-V characteristic studies of AlSb and InSb thin film bilayer structure*, Indian J. Pure & Appl. Phys., 43,5, 383-385, (2005).
11. Sisodia, V., Kabiraj, D., Bolse, W., and Jain, I. P., *Appl. Surf. Sci.*, 252, 1, 4016, (2006).
12. von Muhlen, L., Simao, R. A. and Achete, C. A., *Surface Modification of a-C:H(N) thin films by plasma treatment*, Proceedings of the III LASPM, April 2005.
13. George, J., *Preparation of thin films*, Marcel Dekkar Inc, NY, (1992).
14. Goswami, A., *Thin film fundamentals*, New Age International P. Ltd. Publishers, New Delhi, (1991).
15. Massel, L. I., and Glang, R., *Handbook on thin film technology*, Mc Graw Hill Book Co., NY, (1970).
16. Kasturi Lal Chopra, *Thin film phenomena*, McGraw Hill Book Co., NY, (1969).
17. Holland, L., *Vacuum deposition of thin films*, John Wiley, NY, (1956).
18. Glang, R., *Hand Book of thin film technology*, McGraw Hill, NY, (1970).
19. Kasturi Lal Chopra and Suhit Ranjan Das, *Thin film Solar Cells*, Plenum Press, NY, (1983).
20. Ludmille Eckertove, *Physics of thin films*, Plenum Press, NY, (1986).
21. Dell'oca, C. J., Pulfery, D. L., and Young, L., *Physics of thin films*, Academic Press, NY, (1971).
22. Sakurai, T., and Haye Kawe, S., *J. Appl. Phys.* 13, 1733, (1973).
23. Badour, R. F. and Timmins, R. S., *The Application of plasma to chemical processing*, MIT press, MA, (1967).
24. Francis. F. Chen, *Introduction to plasma physics and controlled fusion*, In: Plasma Physics, Vol. 1, (1974).

25. Sen, S. N., *Plasma physics-plasma state of matter*, Pragati Prakashan, Meerut, 4th edition, (2001).
26. Smirnov, B. M., *Introduction to plasma physics*, Mir publishers, Moscow, (1977).
27. Chanchal Uberoi, *Introduction to un-magnetized plasmas*, Prentice Hall of India P. Ltd., ND, (1997).
28. Microsoft Encarta reference library 2005
29. http://www.apsd.org/plasma_brochure/page5.html, 25th July, 2007
30. Thomas. C. Killian, *Ultra cold neutral plasmas*, Science Magazine, Vol 316, 4, (2007).
31. Leonard C. Feldman and James W. Mayer, *Fundamentals of Surface and thin film analysis*, Elsevier science publishing Comp. Inc., NY, (1986).
32. Mario Birkholz, *Thin film analysis by X-ray scattering*, WILEY-VCH Verlag GmbH & Co. KGaA, Weinheim, (2006).
33. Saskia Kraft, Beate Schattat, Wolfgang Bolse, Siegfried Klaumunzer, Felix Harbsmeier, Agnieszka Kulinska and Anton Loffl, *Ion beam mixing of ZnO/SiO₂ and Sb/Ni/Si interfaces under swift heavy ion irradiation*, J.Appl. Phys., 91, 3, (2002).
34. Pankaj Tyagi and A. G. Vedeshwar, *Grain size dependent optical band gap of CdI₂ films*, Bull. Mater. Sci., 24, 3, 297–300, (2001).
35. Kin Man, A. J. Moll, Ning Chan, W. Walukiewicz and P. Becla, *Substitutionality of Ge atoms in ion implanted AlSb*, Appl. Phys. Lett., 66, 18, (1995).

Bibliography

1. Massel, L. I., *Physics of thin films*, Vol.3 & Vol.4, Academic Press Inc., NY, (1966,1967).
2. Cullity, B. D., *Elements of X-ray Diffraction*, Addison Wesley Publishing Co. Inc., Massachusetts, (1967).

3. Heavens, O. S., *Optical properties of thin films*, Butterworth Scientific Publications, London, (1955).
4. Pallab Bhattacharya, *Semiconductor opto-electronic devices*, Prentice Hall Inc., (1997).
5. Alder van der Ziel, *Solid-state physical electronics*, Prentice Hall of India Pvt. Ltd., (1971).
6. Poate, J. M., Tu, K. N., Mayer, J. W., *Thin films-interdiffusion and reactions*, A Wiley-inter science Pub., (1978).
7. Biswanath Chakkarborthi, *Principles of plasma mechanics*, New Age International P. Ltd, India, (1997).
8. http://www.plasmas.org/rot_plasmas.htm, 25th July 2007.

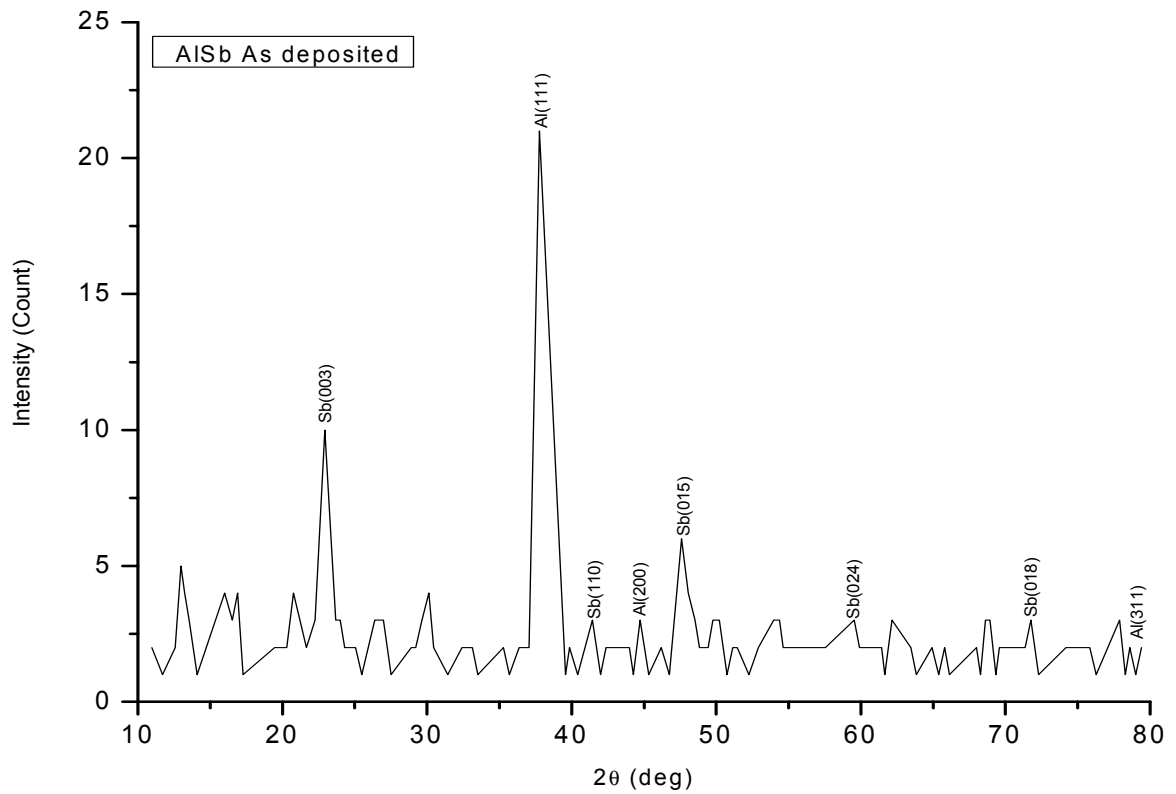


Figure 6.2. X-ray diffraction pattern of as deposited sample.

Table 6.2A Crystal data of as deposited AlSb bilayer thin film

| JCPDS Data | | | Experimental Result | | | Material | Structure |
|------------|-----|--------------------|---------------------|--------------------|----------------|----------|-----------|
| 2θ (deg.) | hkl | d _{hkl} Å | 2θ (deg.) | d _{hkl} Å | β(FWHM) (deg.) | | |
| 23.767 | 003 | 3.74072 | 22.9400 | 3.87368 | 0.4800 | Sb | Hexagonal |
| 38.474 | 111 | 2.33795 | 37.7816 | 2.37919 | 0.3433 | Al | Cubic |
| 41.98 | 110 | 2.15044 | 41.4500 | 2.17671 | 0.1000 | Sb | Hexagonal |
| 47.244 | 015 | 1.92238 | 47.6000 | 1.90883 | 0.3600 | Sb | Hexagonal |
| 59.532 | 024 | 1.55158 | 59.5400 | 1.55140 | 0.1200 | Sb | Hexagonal |
| 71.857 | 018 | 1.37276 | 71.7600 | 1.31430 | 0.0400 | Sb | Hexagonal |
| 78.232 | 311 | 1.22096 | 78.6100 | 1.21604 | 0.1400 | Al | Cubic |

Table 6.2B Cell parameters of as deposited AlSb bilayer thin film

| Material | Cell Parameters | | | | | |
|----------|-----------------|-----|-------|--------------|-----|--------|
| | JCPDS Data | | | Experimental | | |
| | a Å | b Å | c Å | a Å | b Å | c Å |
| Al-cubic | 4.049 | - | - | 4.033 | - | - |
| Sb-Hexa | 4.300 | - | 11.22 | 3.676 | - | 11.621 |

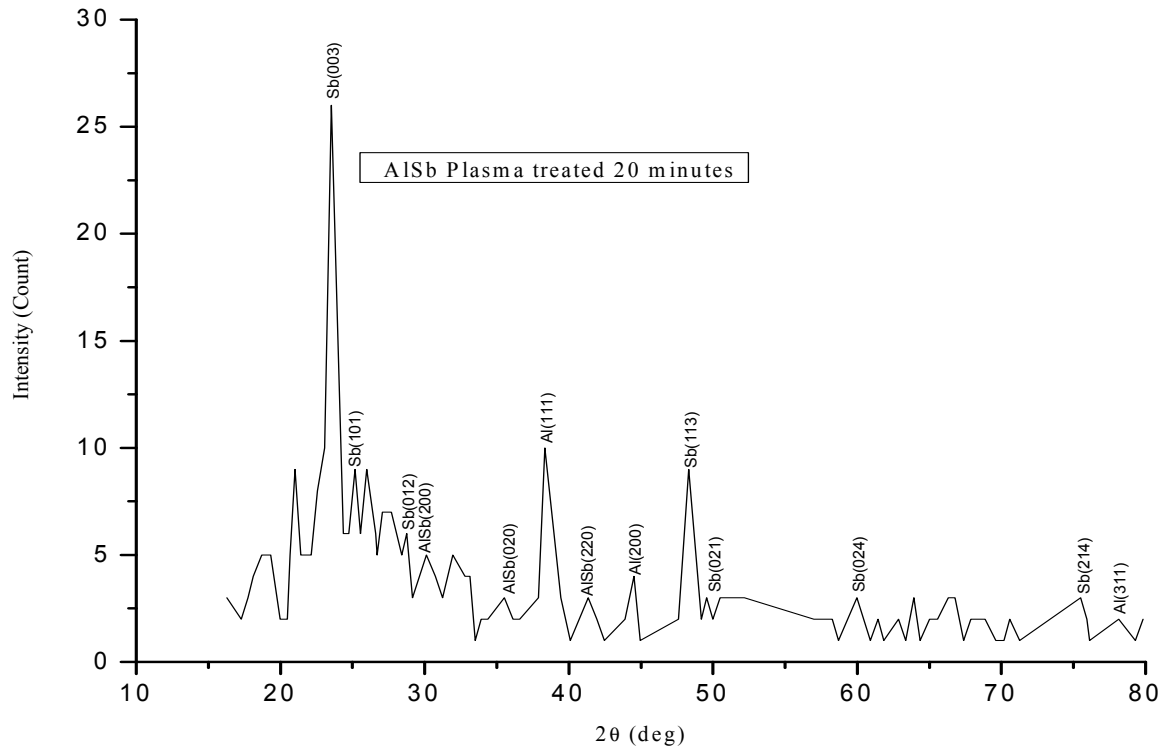


Figure 6.3 X-ray diffraction pattern of sample A

Table 6.3A Crystal data of sample A (plasma treated 20 minutes)

| JCPDS Data | | | Experimental Result | | | Material | Structure |
|------------|-----|--------------------|---------------------|--------------------|----------------|----------|--------------|
| 2θ (deg.) | hkl | d _{hkl} Å | 2θ (deg.) | d _{hkl} Å | β(FWHM) (deg.) | | |
| 23.767 | 003 | 3.74072 | 23.5150 | 3.78024 | 0.5100 | Sb | Hexagonal |
| 25.172 | 101 | 3.53503 | 25.1700 | 3.53531 | 0.2400 | Sb | Hexagonal |
| 28.746 | 012 | 3.10312 | 28.7500 | 3.10270 | 0.1000 | Sb | Hexagonal |
| 29.130 | 200 | 3.06308 | 29.1500 | 3.06103 | 0.0600 | AlSb | Cubic |
| 34.868 | 020 | 2.57103 | 34.3800 | 2.6064 | 0.0400 | AlSb | Orthorhombic |
| 38.474 | 111 | 2.33795 | 38.3400 | 2.34581 | 0.3200 | Al | Cubic |
| 41.666 | 220 | 2.16592 | 41.3600 | 2.18124 | 0.1200 | AlSb | Cubic |
| 44.738 | 200 | 2.02406 | 44.5100 | 2.03391 | 0.1400 | Al | Cubic |
| 48.810 | 113 | 1.86430 | 48.7800 | 1.86538 | 0.4600 | Sb | Hexagonal |
| 49.579 | 021 | 1.83717 | 49.5500 | 1.83818 | 0.1400 | Sb | Hexagonal |
| 59.532 | 024 | 1.55158 | 59.9800 | 1.54107 | 0.0400 | Sb | Hexagonal |
| 75.497 | 214 | 1.25825 | 75.8500 | 1.25328 | 0.1000 | Sb | Hexagonal |
| 78.227 | 311 | 1.22103 | 78.134 | 1.22225 | 0.0400 | Al | Cubic |

Table 6.3B Cell parameters of sample A (plasma treated 20 minutes)

| Material | Cell Parameters | | | | | |
|------------|-----------------|-------|-------|--------------|-------|-----|
| | JCPDS Data | | | Experimental | | |
| | a Å | b Å | c Å | a Å | b Å | c Å |
| AlSb-cubic | 6.126 | - | - | 6.122 | - | - |
| AlSb-Orth | 5.391 | 5.142 | 5.894 | 5.259 | 5.212 | - |

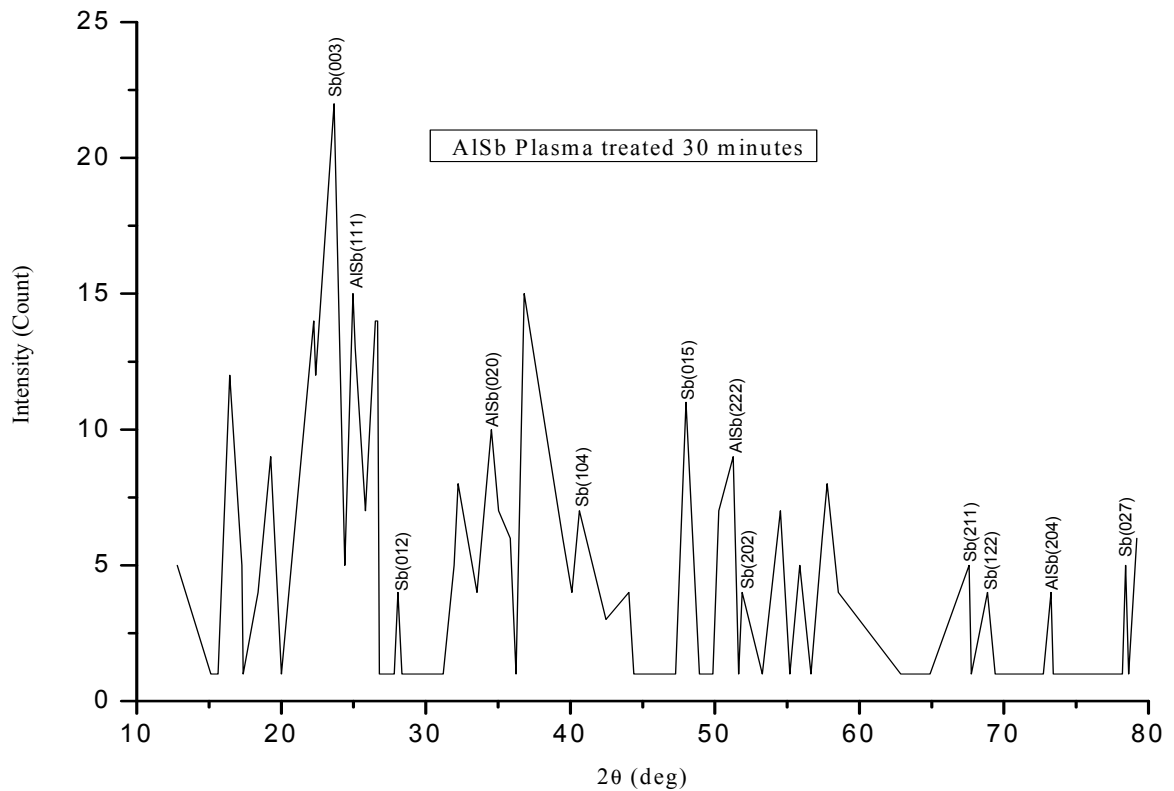


Figure 6.4 X-ray diffraction pattern of sample B (plasma treated 30 minutes)

Table 6.4A Crystal of sample B (plasma treated 30 minutes)

| JCPDS Data | | | Experimental Result | | | Material | Structure |
|------------|-----|--------------------|---------------------|--------------------|----------------|----------|--------------|
| 2θ (deg.) | hkl | d _{hkl} Å | 2θ (deg.) | d _{hkl} Å | β(FWHM) (deg.) | | |
| 23.767 | 003 | 3.74072 | 23.6566 | 3.75794 | 0.0433 | Sb | Hexagonal |
| 25.158 | 111 | 3.53696 | 25.1046 | 3.54437 | 0.0593 | AlSb | Cubic |
| 28.746 | 012 | 3.10312 | 28.067 | 3.17664 | 0.0800 | Sb | Hexagonal |
| 34.868 | 020 | 2.57103 | 34.5433 | 2.59446 | 0.0733 | AlSb | Orthorhombic |
| 40.209 | 104 | 2.24098 | 40.1133 | 2.24611 | 0.0933 | Sb | Hexagonal |
| 47.244 | 015 | 1.92238 | 47.969 | 1.89501 | 0.0607 | Sb | Hexagonal |
| 51.644 | 222 | 1.76845 | 51.8950 | 1.76049 | 0.1300 | AlSb | Cubic |
| 51.674 | 202 | 1.76750 | 51.2733 | 1.78037 | 0.0800 | Sb | Hexagonal |
| 66.935 | 211 | 1.39682 | 67.623 | 1.38428 | 0.08670 | Sb | Hexagonal |
| 68.684 | 122 | 1.36546 | 68.8600 | 1.3624 | 0.0800 | Sb | Hexagonal |
| 73.327 | 204 | 1.29004 | 73.2500 | 1.29120 | 0.0600 | AlSb | Orthorhombic |
| 78.691 | 027 | 1.21499 | 78.4100 | 1.21864 | 0.0600 | Sb | Hexagonal |

Table 6.4B Cell parameters of sample B (plasma treated 30 minutes)

| Material | Cell Parameters | | | | | |
|------------|-----------------|-------|-------|--------------|------|------|
| | JCPDS Data | | | Experimental | | |
| | a Å | b Å | c Å | a Å | b Å | c Å |
| AlSb-cubic | 6.126 | - | - | 6.139 | - | - |
| AlSb-Orth | 5.391 | 5.142 | 5.894 | 5.34 | 5.19 | 5.90 |

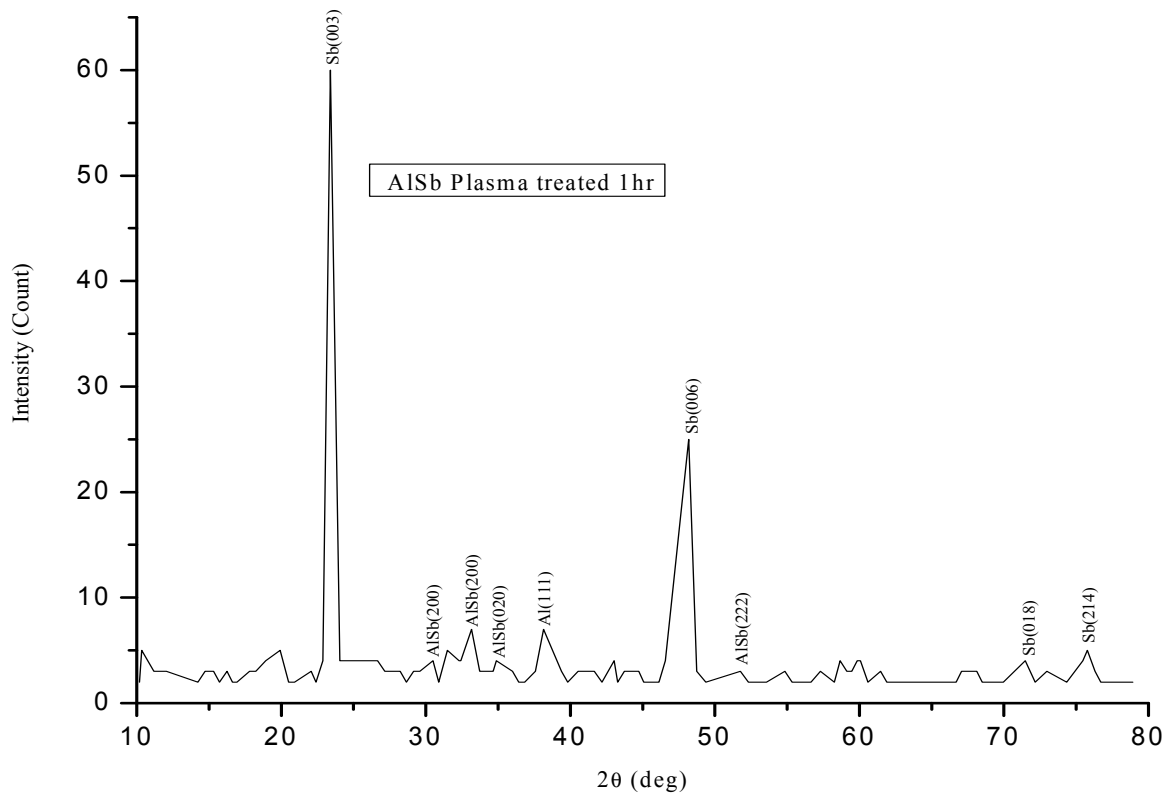


Figure 6.5 X-ray diffraction pattern of sample C (plasma treated 60 minutes)

Table 6.5A Crystal data of sample C (plasma treated 60 minutes)

| JCPDS Data | | | Experimental Result | | | Material | Structure |
|------------|-----|--------------------|---------------------|--------------------|----------------|----------|--------------|
| 2θ (deg.) | hkl | d _{hkl} Å | 2θ (deg.) | d _{hkl} Å | β(FWHM) (deg.) | | |
| 23.767 | 003 | 3.74072 | 23.3995 | 3.79864 | 0.3876 | Sb | Hexagonal |
| 29.130 | 200 | 3.06308 | 29.1700 | 3.05898 | 0.1000 | AlSb | Cubic |
| 33.178 | 200 | 2.69803 | 33.1800 | 2.69787 | 0.1200 | AlSb | Orthorhombic |
| 34.868 | 020 | 2.57103 | 34.8800 | 2.57018 | 0.0800 | AlSb | Orthorhombic |
| 38.472 | 111 | 2.33806 | 38.1400 | 2.35765 | 0.3600 | Al | Cubic |
| 48.641 | 006 | 1.87038 | 48.1767 | 1.88732 | 0.4600 | Sb | Hexagonal |
| 51.644 | 222 | 1.76846 | 51.794 | 1.76369 | 0.1400 | AlSb | Cubic |
| 71.857 | 018 | 1.31276 | 71.4700 | 1.31892 | 0.2200 | Sb | Hexagonal |
| 75.497 | 214 | 1.25825 | 75.4750 | 1.25857 | 0.2300 | Sb | Hexagonal |

Table 6.5B Cell parameters of sample C (plasma treated 60 minutes)

| Material | Cell Parameters | | | | | |
|-----------|-----------------|-------|-------|--------------|------|-----|
| | JCPDS Data | | | Experimental | | |
| | a Å | b Å | c Å | a Å | b Å | c Å |
| AlSb-Cub | 6.126 | - | - | 6.104 | - | - |
| AlSb-Orth | 5.391 | 5.142 | 5.894 | 5.395 | 5.14 | - |

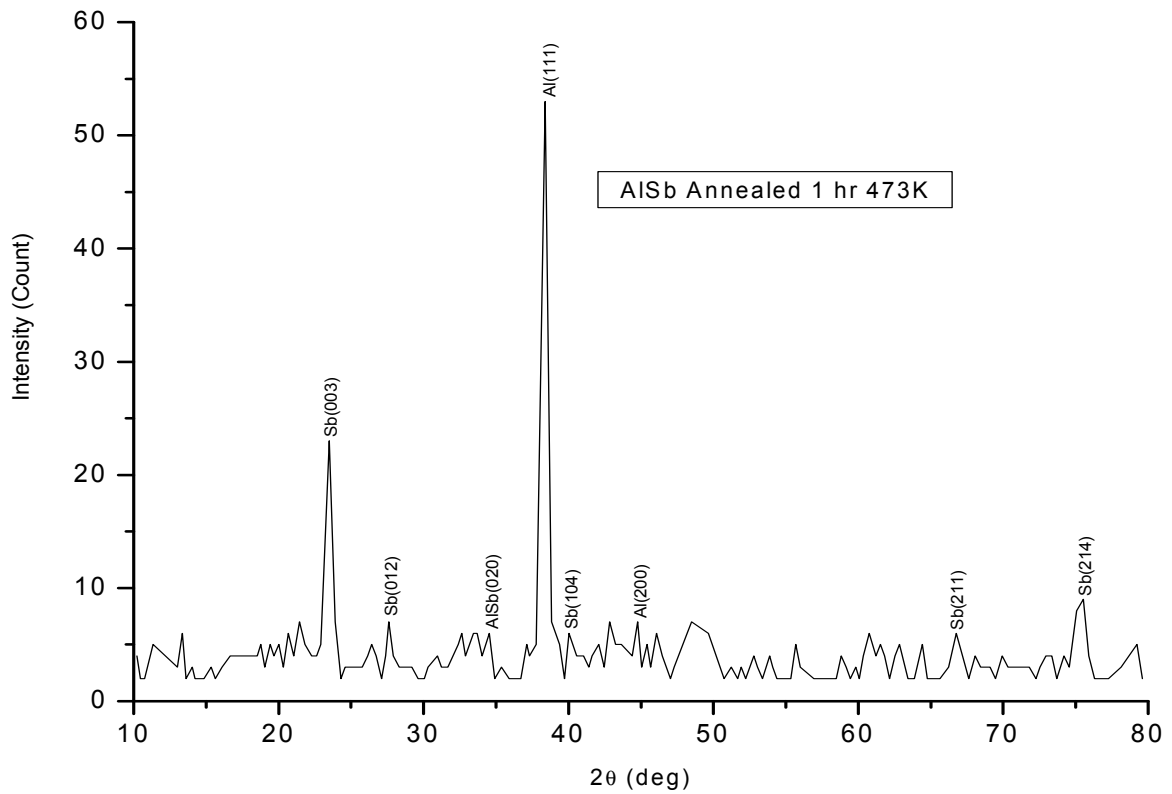


Figure 6.6 X-ray diffraction pattern of sample D

Table 6.6A Crystal of sample D (annealed 60minutes 473K)

| JCPDS Data | | | Experimental Result | | | Material | Structure |
|------------|-----|--------------------|---------------------|--------------------|----------------|----------|--------------|
| 2θ (deg.) | hkl | d _{hkl} Å | 2θ (deg.) | d _{hkl} Å | β(FWHM) (deg.) | | |
| 23.767 | 003 | 3.74072 | 23.5016 | 3.78237 | 0.3367 | Sb | Hexagonal |
| 28.746 | 012 | 3.10312 | 27.6150 | 3.22760 | 0.0900 | Sb | Hexagonal |
| 34.868 | 020 | 2.57103 | 34.5300 | 2.59542 | 0.1800 | AlSb | Orthorhombic |
| 38.474 | 111 | 2.33795 | 38.3880 | 2.34299 | 0.3520 | Al | Cubic |
| 40.209 | 104 | 2.24098 | 40.0300 | 2.25059 | 0.1400 | Al | Cubic |
| 44.722 | 200 | 2.02475 | 44.7816 | 2.02220 | 0.1033 | Sb | Hexagonal |
| 66.935 | 211 | 1.39682 | 66.7633 | 1.4000 | 0.1267 | Sb | Hexagonal |
| 75.497 | 214 | 1.25826 | 75.5200 | 1.25793 | 0.1200 | Sb | Hexagonal |

Table 6.6B. Cell parameters of sample D (annealed 60minutes 473K)

| Material | Cell Parameters | | | | | |
|-----------|-----------------|-------|-------|--------------|-------|-----|
| | JCPDS Data | | | Experimental | | |
| | a Å | b Å | c Å | a Å | b Å | c Å |
| AlSb-Orth | 5.391 | 5.142 | 5.894 | - | 5.190 | - |

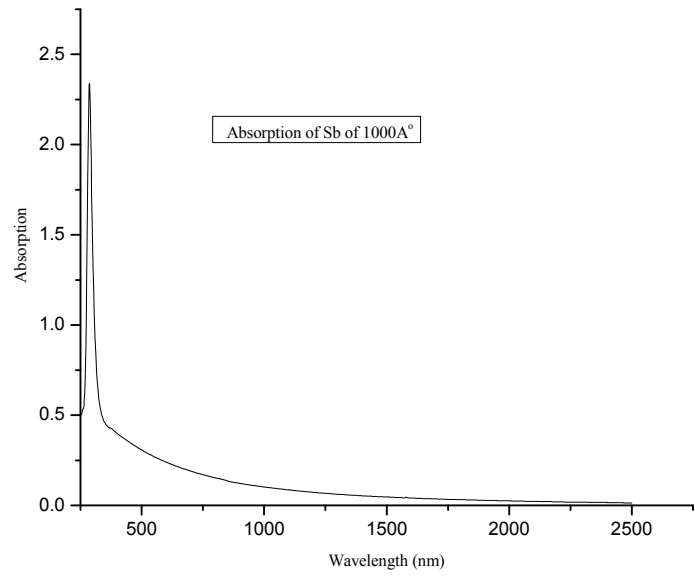


Figure 6.7 Optical absorption spectra of spectra as deposited Sb thin film.

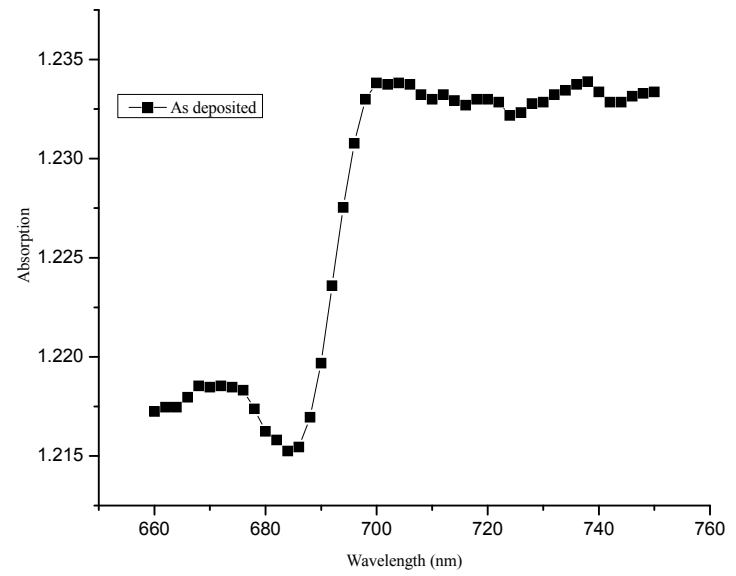


Figure 6.8 Optical absorption of as deposited AlSb thin film

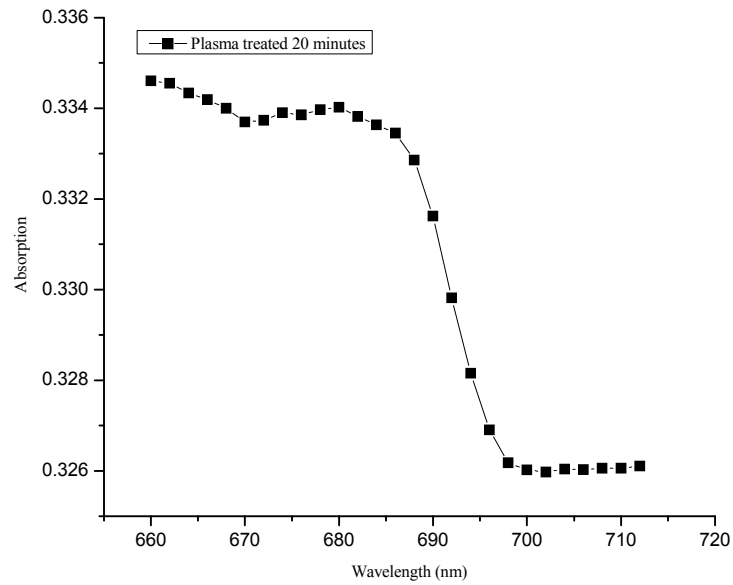


Figure 6.9A Optical absorption spectra of sample A (plasma treated 20 min) $(h\nu)^{1/2}$ for treated 20 min)

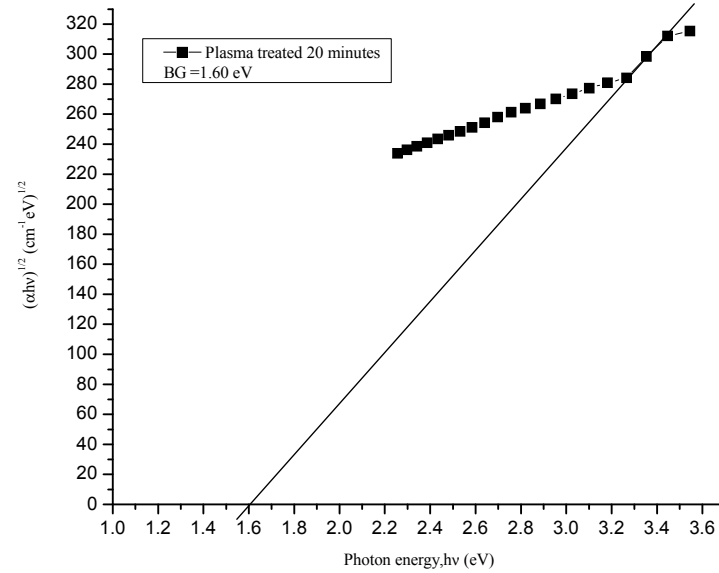


Figure 6.9B Photon energy ($h\nu$) vs $(\alpha h\nu)^{1/2}$ for indirect band gap of sample A ((plasma treated 20 min) BG=1.60 eV)

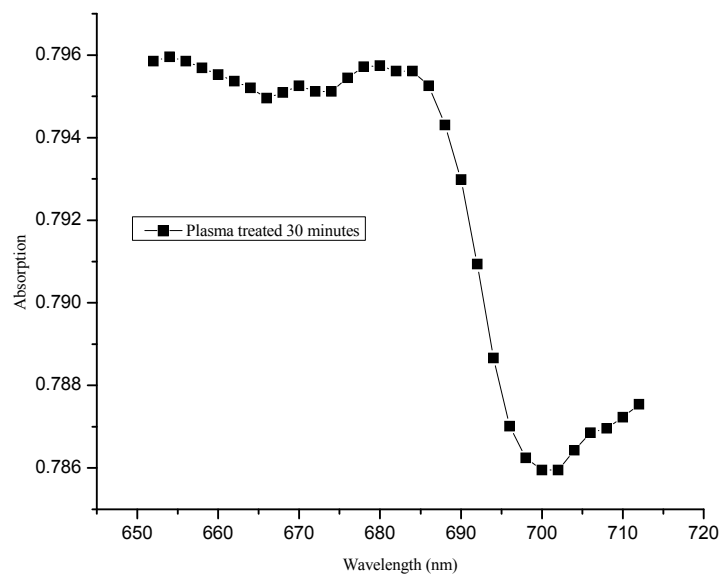


Figure 6.10A Optical absorption spectra of sample B (plasma treated 30 min treated 30 min)

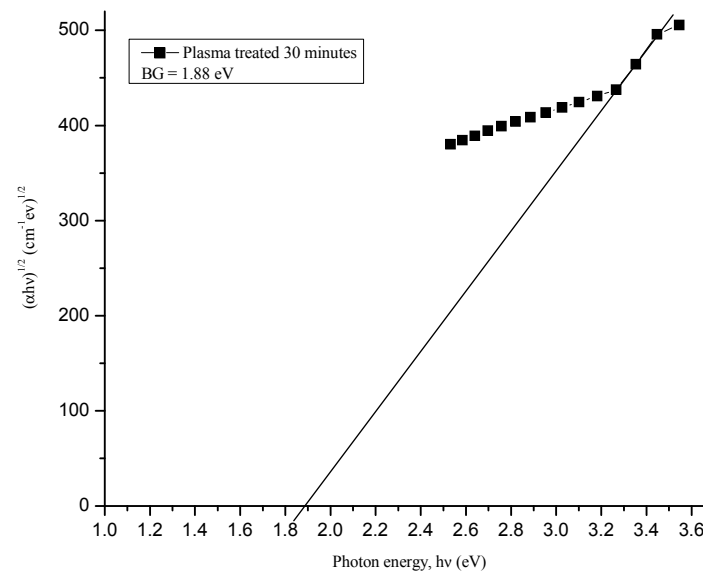


Figure 6.10B Photon energy ($h\nu$) vs $(\alpha h\nu)^{1/2}$ for indirect band gap of sample B (plasma treated 30 min)

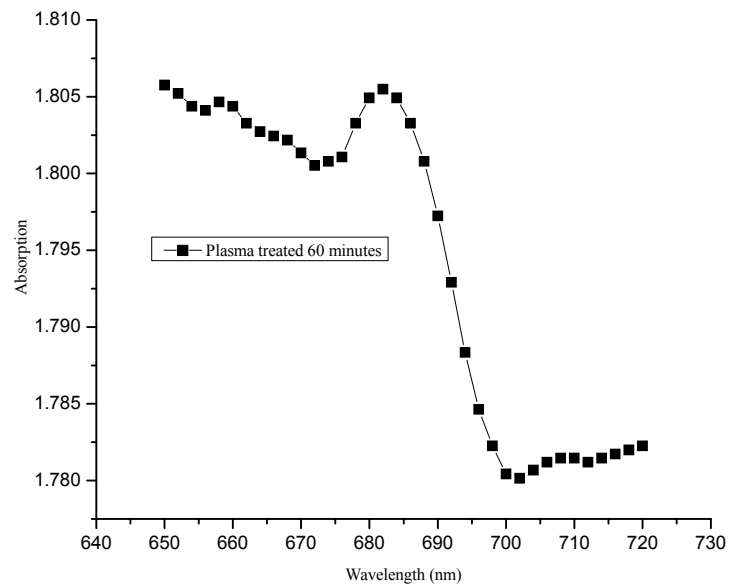


Figure 6.11A Optical absorption spectra of
 $(\alpha h\nu)^{1/2}$ for sample C (plasma treated 60 min)
 treated 60 min)

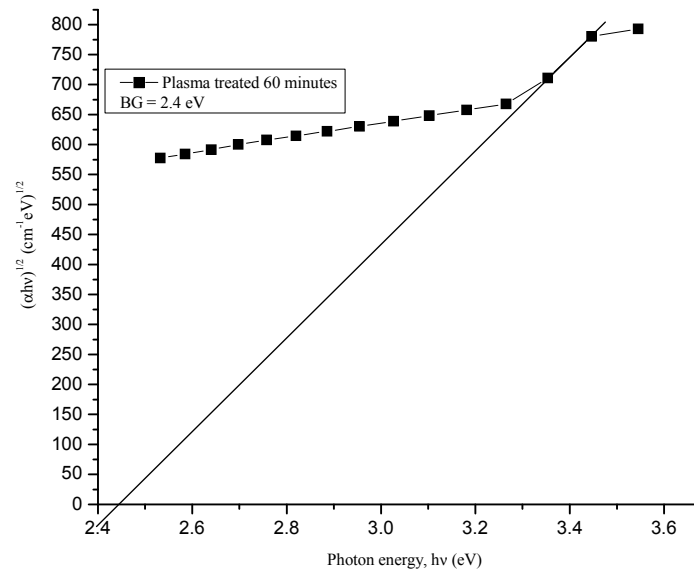


Figure 6.11B Photon energy ($h\nu$) vs
 indirect band gap of sample C (plasma
 treated 60 min)

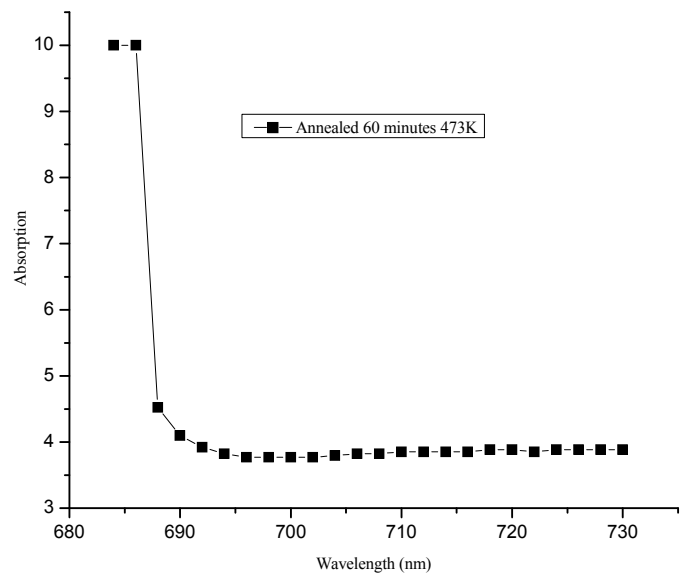


Figure 6.12A Optical absorption spectra of $(\alpha h\nu)^{1/2}$ for sample D (annealed 60 min 473K) (annealed 60 min 473K)

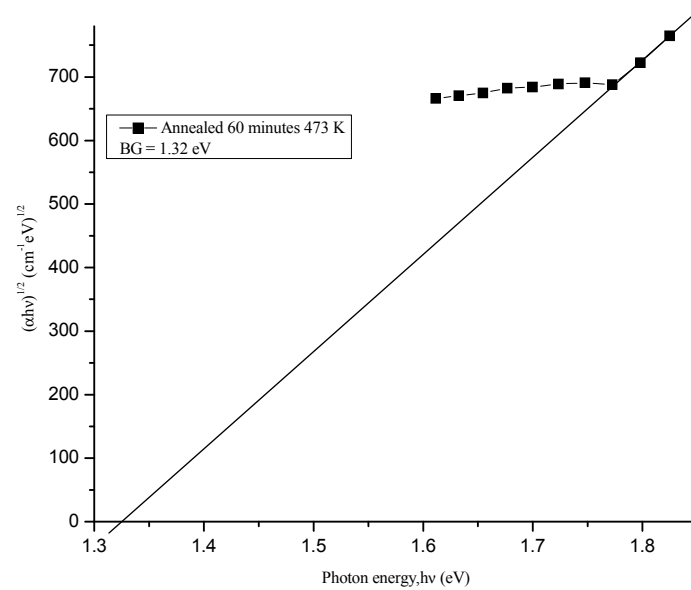


Figure 6.12B Photon energy ($h\nu$) vs indirect band gap of sample D

Table 6.7. Structural parameters and band gap energy of the newly formed AlSb compound

| Sample | Grain size D_c (nm) | Grain size D_o (nm) | δ_c $\times 10^{14}$ m^{-2} | δ_o $\times 10^{14}$ m^{-2} | ϵ_c $\times 10^{-4}$ | ϵ_o $\times 10^{-4}$ | Band Gap (eV) |
|-----------------------------|-----------------------------|-----------------------------|--|--|----------------------------------|----------------------------------|---------------------|
| Plasma treated 20 min | 142.88774 | 217.13357 | 0.4898 | 0.2121 | 2.5347 | 1.6680 | 1.60 |
| Plasma treated 30 min | 70.98114 | 118.54274 | 1.9848 | 0.7116 | 5.1024 | 3.0552 | 1.88 |
| Plasma treated 60 min | 65.58828 | 108.71457 | 2.3459 | 0.8461 | 5.4973 | 3.3314 | 2.4 |

Annealed Sample

| | | | | | | | |
|-----------------------------|---|----------|---|--------|---|---------|------|
| Annealed 60 min 473 K | - | 48.27150 | - | 4.2916 | - | 41.6832 | 1.32 |
|-----------------------------|---|----------|---|--------|---|---------|------|

- D_c = Grain size of the cubic structure,
- D_o = Grain size of the orthorhombic structure
- δ_c = Dislocation density of the cubic structure,
- δ_o = Dislocation density of the orthorhombic structure,
- ϵ_c = Micro strain on the cubic structure,
- ϵ_o = Micro strain on the orthorhombic structure.



Figure 3.1 HIND HI VACUUM Coating Unit



Figure 5.1 Plasma Chamber